

**Efficient Low-Power Remote Sensing System Design for Embedded  
Guided Wave Ultrasonic Structural Health Monitoring of Aerospace  
Structures using Wireless Sensor Networks**

By

**Taha Ali**

2011-NUST-MS PhD-Elec (Comm-N)-16



Supervised by

**Cdr. Dr. Tariq Mairaj Rasool Khan PN**

A dissertation submitted to

PAKISTAN NAVY ENGINEERING COLLEGE  
NATIONAL UNIVERSITY OF SCIENCES AND TECHNOLOGY, ISLAMABAD

in partial fulfillment of the requirements for the degree of

**MS ELECTRICAL ENGINEERING (COMMUNICATIONS)**

November 2014

Thesis Title:

**Efficient Low-Power Remote Sensing System Design for Embedded Guided Wave Ultrasonic Structural Health Monitoring of Aerospace Structures using Wireless Sensor Networks**



Thesis submitted in partial fulfillment of the requirements for the degree of Master of Science in Electrical Engineering with specialization in Communications to the Department of Electronics and Power Engineering at PNEC-NUST.

Submitted by:

Taha Ali

Reg. No. 2011-NUST-MS PhD-Elec (Comm-N)-16

Supervised by:

Cdr. Dr. Tariq Mairaj Rasool Khan PN

Assistant Professor

Department of Electronics and Power Engineering

Guidance and Examination Committee:

1. Cdr. Dr. Faisal Amir PN, Assistant Professor (EPE)
2. Lt. Cdr. Dr. Aqueel Shah PN, Assistant Professor (IME)
3. Dr. Sameer Hashmat Qazi, Assistant Professor (EPE)


# National University of Sciences and Technology

## MASTER'S THESIS WORK

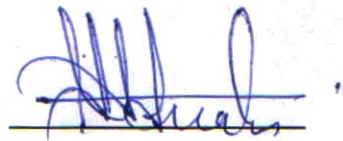
We hereby recommend that the dissertation prepared under our supervision by: Taha Ali (2011-NUST-MS PhD-Elec (Comm-N)-16) titled: "Efficient low-power remote sensing system design for embedded guided wave ultrasonic structural health monitoring of aerospace structures using wireless sensor networks" be accepted in partial fulfillment of the requirements for the award of MS Electrical Engineering (Communications) degree.

### Examination Committee Members


1. Name: Cdr. Dr. Faisal Amir PN

Signature: 

2. Name: Lt. Cdr. Dr. Aqueel Shah PN

Signature: 

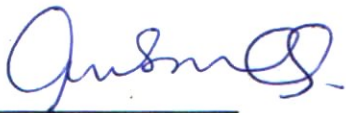
3. Name: Dr. Sameer Hashmat Qazi

Signature: 

Supervisor's name: Cdr. Dr. Tariq Mairaj Rasool Khan PN

Signature: 

Date: 07 Nov 2014



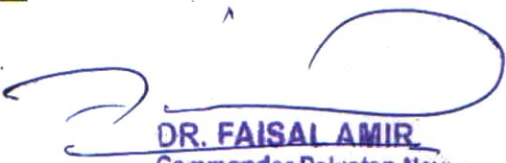
Head of Department

11/11/2014

Date

### COUNTERSIGNED

Date: 19/11/2014

  
**DR. FAISAL AMIR**  
 Commander Pakistan Navy  
 Dean/Principal  
 Power Engg  
**PNS JAUHAR**

# **Dedication**

Dedicated to my beloved parents

## **Acknowledgments**

First and foremost, I would like to thank Allah Almighty, the Creator of this universe, the most Gracious, the most Merciful, the Omniscient, Who bestowed me the knowledge, and the strength to learn, grasp and apply it for completing this dissertation.

I am extremely grateful to my thesis supervisor cum mentor Cdr. Dr. Tariq Mairaj Rasool Khan PN, whose able guidance, consistent encouragement, and motivation aided me to achieve this honor. I would like to specially appreciate his patience for my faults, his sacrifice for time when required, and his expert opinions in difficult times. In fact, this endeavor could not be completed without him. I would also like to express my gratitude for the G.E.C. members: Dr. Faisal Amir for consistent motivation and advices, Dr. Aqueel Shah for help in acquiring IME lab facilities, and Dr. Sameer Qazi for critically reviewing this dissertation.

I would like to gratefully acknowledge all the support from NDT Research Center, PNEC-NUST, and its honorable members. In particular, Mr. Junaid Muzammil and Mr. Taha Saeed Khan have been a constant support in carrying out different activities, and stimulating useful discussions. Junaid's motivational support is also acknowledged.

Finally, I am thankful to my family members, whose constant support and encouragement enabled me to achieve this enormous task. I have no words to describe their unwavering support and inexhaustible tolerance. I also pay reverence to my parent's prayers and my sibling's love for me, which will remain a source of endurance for the rest of my life.

# Table of Contents

Approval Page.....	2
Dedication.....	3
Acknowledgments.....	4
Table of Contents.....	5
List of Figures.....	7
List of Tables.....	9
List of Abbreviations.....	10
Abstract.....	11
Chapter 1 Introduction.....	13
1.1 Background and motivation.....	13
1.1.1 Non-Destructive Testing.....	16
1.1.2 Guided Wave Ultrasonic Testing.....	17
Pros and Cons.....	18
Applications and prospects in Pakistan.....	19
1.1.3 Structural Health Monitoring.....	21
1.1.4 Wireless Sensor Networks.....	21
1.2 Research Objectives.....	22
1.2.1 GWUT based wireless SHM.....	22
1.2.2 Objectives.....	23
1.3 Dissertation Outline.....	23
Chapter 2 Literature Review.....	25
2.1 Relevant Work.....	25
2.2 Contemporary solutions for GWUT based SHM.....	26
2.3 Limitations of current solutions.....	29
2.4 Problem statement – Thesis.....	30
Chapter 3 Guided Wave Ultrasonic Testing Theory.....	31
3.1 Waves.....	31
3.1.1 Lamb waves and Guided waves.....	32
Modes.....	33
Dispersion.....	34

3.2	Generating Guided waves .....	36
3.2.1	Transducers used for exciting Guided waves .....	37
3.2.2	Generating Guided waves using piezoelectric transducers .....	38
3.2.3	Role of couplant .....	39
3.3	Guided Wave Ultrasonic Testing.....	40
3.3.1	Configuration modes for GWUT .....	40
3.3.2	Localization using GWUT .....	41
Chapter 4	Experiments .....	42
4.1	Selection of specimen, transducers and couplant .....	42
4.2	Experimental Setup.....	43
4.2.1	Excitation .....	43
4.2.2	Positioning .....	44
4.2.3	Methodology.....	45
4.3	Design of Instrumentation Amplifier and Envelope Detector – The Signal Conditioning Circuit .....	46
4.3.1	Pre-amplifier design.....	47
4.3.2	Envelope detector design .....	49
	Precision full-wave rectifier design .....	50
	Low-pass active filter design .....	52
4.4	Data Acquisition and Transmission over TelosB using TinyOS.....	55
4.4.1	Implementation over NesC and TinyOS.....	56
4.4.2	ADC configuration for TelosB .....	58
4.4.3	Wave capture and buffering.....	61
4.4.4	Communication protocol and packet format.....	61
4.4.5	Program structure for remote station .....	64
4.4.6	Program structure for base station .....	66
4.5	Signal Processing at the Base Station.....	69
4.6	Results.....	70
Chapter 5	Discussion and Future Work.....	73
5.1	Defense of Thesis – Comparison with Contemporary work.....	73
5.2	Limitations .....	75
5.3	Conclusion .....	76
5.4	Summary of Contributions.....	77
5.5	Recommendations for future work .....	77
References	.....	79

## List of Figures

Figure 1-1: Aloha Airlines Flight-243 disaster .....	14
Figure 1-2: Bulk waves for UT versus lamb waves for GWUT .....	18
Figure 3-1: Lamb wave mode families .....	34
Figure 3-2: Lamb wave phase velocity dispersion curve for Al6061, 2a=10mm, 2d=2mm .....	35
Figure 3-3: Lamb wave group velocity dispersion curve for Al6061, 2a=10mm, 2d=2mm .....	35
Figure 3-4: Lamb wave generation using Snell's law .....	36
Figure 3-5: Lamb wave generation through surface pinching .....	37
Figure 3-6: Correct electrical alignment for PZT wafers.....	39
Figure 3-7: Pitch-catch configuration .....	40
Figure 3-8: Pulse-echo configuration: with single transducer (shown atop), with pair (bottom). 41	
Figure 4-1: PZT-5A equivalent (P33) transducers (unused, + sign indicates positive electrode) 42	
Figure 4-2: Modulated Gaussian pulse as the excitation signal.....	44
Figure 4-3: Position of transducers on the specimen, top view (not to scale) .....	45
Figure 4-4: Received signal from sensor PZT without crack .....	46
Figure 4-5: Received signal from sensor PZT with crack .....	46
Figure 4-6: Sensing chain for wireless GWUT-SHM.....	47
Figure 4-7: Instrumentation amplifier based pre-amplifier for sensing.....	48
Figure 4-8: Response of pre-amplifier.....	49
Figure 4-9: Ideal envelope detector circuit .....	50
Figure 4-10: Output of precision rectifier for envelope extraction.....	51
Figure 4-11: Precision rectifier circuit.....	51
Figure 4-12: Low pass active filter circuit for envelope detector .....	53
Figure 4-13: Final output of the signal conditioning circuit .....	53
Figure 4-14: Complete test setup with signal conditioning circuit.....	54
Figure 4-15: PCB layout design for the Signal Conditioning Circuit (SCC) .....	54
Figure 4-16: Wireless SHM setup.....	56
Figure 4-17: A component graph of a TinyOS application configuration in Yeti2.....	58
Figure 4-18: A component graph with module interfaces shown.....	58
Figure 4-19: Saw-tooth wave sampled without DMA .....	60
Figure 4-20: Saw-tooth wave sampled with DMA.....	60
Figure 4-21: GWUT acquisition file format .....	62
Figure 4-22: GWUT data packet (sequence) .....	63
Figure 4-23: Protocol sequence diagram implemented for Single-hop communication .....	63
Figure 4-24: GWUT command and acknowledgement packet.....	64
Figure 4-25: State diagram for wireless mote at RS .....	65
Figure 4-26: Transmission flow chart at RS mote .....	66
Figure 4-27: State diagram for BS mote .....	67
Figure 4-28: Flowchart for reception at BS mote .....	68
Figure 4-29: GWUT waveform acquired at BS .....	69
Figure 4-30: GWUT waveform after interpolation at BS .....	69
Figure 4-31: Reference signal (healthy) after registration.....	70
Figure 4-32: Signal Healthy-1 compared with reference at BS .....	71



Figure 4-33: Signal Healthy-2 compared with reference at BS .....	71
Figure 4-34: Signal Flawed-1 compared with reference at BS .....	71
Figure 4-35: Signal Flawed-2 compared with reference at BS .....	72

## **List of Tables**

Table 1: Relative energies of difference between windowed reference and target signals .....	72
Table 2: Comparison with state-of-the-art wireless GWUT-SHM systems .....	74

## List of Abbreviations

AE	Acoustic Emission	PRF	Pulse Repetition Frequency
BS	Base Station	PRI	Pulse Repetition Interval
ET	Eddy current Testing	PZT	Lead Zirconate Titanate
IA	Instrumentation Amplifier	RAM	Random Access Memory
MT	Magnetic Testing	RFT	Remote Field Testing
OT	Optical Testing	SAR	Successive Approximation Register
PT	Penetrant Testing	SCC	Signal Conditioning Circuit
RF	Radio Frequency	SHM	Structural Health Monitoring
RS	Remote Station	S/H	Sample and Hold (circuit)
RT	Radiographic Testing	TIR	Total Internal Reflection
RX	Receiver	UCB	University of California, Berkeley
TX	Transmitter	USC	University of South Carolina
UT	Ultrasonic Testing	WSN	Wireless Sensor Networks
VT	Visual Testing	CMRR	Common Mode Rejection Ratio
$\mu$ C	Microcontroller	EMAT	Electro-Magnetic Acoustic Transducer
$\mu$ P	Microprocessor	EUSR	Embedded Ultrasonic Structural Radar
ADC	Analog to Digital Converter	GWUT	Guided Wave Ultrasonic Testing
AFG	Arbitrary Function Generator	IVHM	Integrated Vehicle Health Management
AML	Active Message Layer	MCLK	Master CLock
DSP	Digital Signal Processor	PVDF	Poly-Vinylidene-Fluoride
FEM	Finite Element Modeling	PWAS	Piezoelectric Wafer Active Sensor
HAL	Hardware Abstraction Layer	NTSB	National Transport and Safety Board
HIL	Hardware Interface Layer	RMSE	Root Mean Square Error
HPL	Hardware Presentation Layer	STXC	Short Time Cross Correlation
IRT	InfraRed (thermal) Testing	SRAM	Static Random Access Memory
NDE	Non-Destructive Evaluation	LRUT	Long Range Ultrasonic Testing
NDT	Non-Destructive Testing	LAMSS	Laboratory for Active Materials and Smart Structures
PSR	Power Supply Rejection ratio		

## **Abstract**

Various engineering structures develop defects and flaws over time due to environmental effects, overloading, wear and tear, fatigue, corrosion and other unavoidable degradations. These flaws pose risk of failure to the whole system, especially when a component is approaching its designed life. In particular, aerospace systems rely heavily on the structural components, and their damage often leads to catastrophic failures. Conventionally, Eddy current Testing (ET) and Ultrasonic Testing (UT) is carried out in aerospace sectors, which require detaching the components in most cases. Research is being carried out in aerospace sectors to examine large areas using few transducers. Guided Wave Ultrasonic Testing (GWUT) has recently evolved as a feasible in-situ testing technique for most structures. However, for continuous GWUT based Structural Health Monitoring (SHM), Wireless Sensor Networks (WSN) need to be deployed. But higher excitation and operating frequencies, high sampling rates, large data volumes, and complex processing increase the cost and power consumption; rendering various WSN platforms infeasible. To meet such stringent constraints, the solutions previously reported tend to use more power hungry platforms. This work proposes a complete remote sensing solution featuring a novel signal conditioning circuit design, which enables low-power, low-cost sensing for wireless GWUT based SHM systems. The circuit is designed to sense, pre-amplify and extract the envelope of the GWUT signal. The extracted signal is then transmitted wirelessly using a low-power zigbee mote over custom designed application protocol. At the Base station, the signal is reconstructed and processed to detect and localize flaws, by comparing against a reference signal. Thus, a detailed remote sensing system design is presented for a wireless GWUT based SHM system.

**Keywords:** Guided wave ultrasonic testing, Remote sensing, Structural health monitoring, Wireless sensor networks, Analog circuits, Instrumentation, Acoustic testing, Piezoelectric transducers, Efficient system design.

# Chapter 1 Introduction

---

## 1.1 Background and motivation

After the on-set of the industrial revolution, verification and inspection methods of industrial machines and structures were evolved. Later, with the increase in demand for reliability, service-life, safety and robustness of engineering structures, not only these methods were improved, new advanced methods for inspection were also sought. The research into new methods penetrated through all engineering disciplines, and all known physical principals were evaluated for their use in testing of materials and structures. This research also focuses on the interdisciplinary area, where mechanical waves in an elastic plate are used to detect flaws using piezoelectric transducers.

The motivation for conducting research in this area comes from different sectors where continuous monitoring of structures is required. The importance of civil infrastructure and primarily transport infrastructure in promoting economic development has been widely recognized among policymakers and economists. The economic impacts of highway infrastructure have been assessed in many countries, and existing studies supports a strong conclusion that the development of highway infrastructure has had significant positive impacts on nation's economic performance. Roads and bridges (highway infrastructure) are among the most important public assets in many countries. Highway infrastructure improvements bring immediate and sometimes dramatic benefits to road users through improved access to hospitals, schools, and markets; improved comfort, speed, and safety; and lower vehicle operating costs. Moreover, other civil structures like energy infrastructure and water management infrastructure

are also key facilities, and have unarguably direct impact on nation's development and economy. For instance, oil and gas pipelines (energy infrastructure) provide uninterrupted energy supply to the industry, whereas flood embankments prevent rivers to flood nearby areas during flooding or rainy season. Therefore, deteriorating bridges, weakening embankments and debilitating pipelines can not only cause life-damages but also severely upset the economical development of a nation. Thus, continuous testing and verification of these structures is a subject of global importance.

Many incidents in aerospace history are also attributed to failure in verification or testing of structural components, especially after maintenance. Fatigue, overloading and corrosion often contribute to development of flaws in aircraft structures. Therefore, many structural components need to be detached for regular inspection. This not only increases down-time, but also increases chances of human error. For instance, in a famous incident to Flight 243 of Aloha Airlines on 28 April 1988, a major portion of the fuselage was ripped off during flight, shown in Figure 1-1.

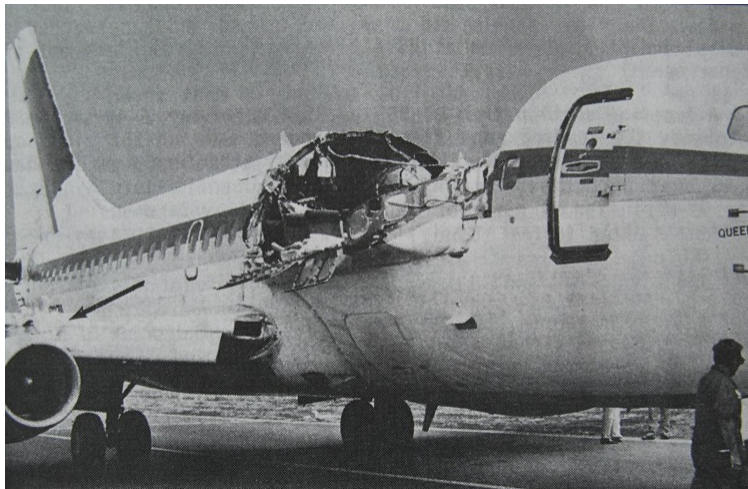


**Figure 1-1: Aloha Airlines Flight-243 disaster<sup>1</sup>**

The investigation revealed that the accident was a result of fatigue in fuselage panels accelerated by corrosion. Though only one fatal casualty was reported, this is one of the

---

<sup>1</sup> © Public Domain: Downloaded from Wikimedia, Work of NTSB released for Public Domain, [here](#).

incidents that formed the basis of strict testing methods in aerospace industry. However, other incidents such as that of Japan flight 123 in 1985 and china flight 611 in 2002 were also reported as lack in testing and verification capabilities. Both incidents were fatal, with four and zero survivors respectively, and both were due to fatigue in bulk head.

Research is being carried out in continuous monitoring called Structural Health Monitoring (SHM) of civil and aerospace structures [1,2,3,4,5]. Many Non-Destructive Testing (NDT) techniques currently in use are not suitable for SHM. For example, Eddy current Testing (ET) and Ultrasonic Testing (UT) are currently major NDT techniques used by the aircraft industry. ET needs movement of probe over the area under test; whereas UT needs direct access to the area under test. Guided Wave Ultrasonic Testing (GWUT) as well as Acoustic Emission (AE) testing techniques can be used in such scenarios to examine a large area using few transducers called in-situ (or in-place) testing, and also locate possible or existing faults. These techniques accompanied with Wireless Sensing Networks (WSN) can be deployed to continuously monitor a particular structure avoiding massive cabling between the sensors and On-Board Computers or Base Station.

Another motivation for this research is to introduce and improve SHM for various kinds of civil infrastructure in Pakistan which has many significant impacts on both the industry and the society. Developed countries are already benefitting from their SHM programs by reduced maintenance costs and failure down time. It is also vital for developing countries like Pakistan where a significant part of the development budget is spent on re-developing damaged infrastructure and its corrective maintenance.

Guided Wave Ultrasonic Testing is a modern state-of-the-art NDT Technique that is now being successfully applied in the modern world. The unique features that make this the method



of choice are its simplicity, cost effectiveness and data acquisition using low power devices with reasonable accuracy. Moreover, this technique can detect the fault at its onset – after the very formation of a hairline crack. In the long run, with appropriate databases developed, SHM accompanied with prognosis algorithms can provide schedules for preventive maintenance thereby reducing maintenance costs and risk of failure. Another significant impact would be the domestic industry becoming aware of NDT Techniques in general and adopting them for a safer, stable and successful Pakistan.

### ***1.1.1 Non-Destructive Testing***

Non-Destructive Testing (NDT) is formally defined as any testing technique that at least detects flaws in a material without effectively damaging it. The material may belong to any structure, machine or any unit of industrial, social or economical importance. The technique must not alter any properties of the unit under test that may affect the parent system's performance. Non-Destructive Evaluation (NDE) is a quantitative version of NDT where the flaws are localized and characterized, such as to estimate flaw shape or size. Perhaps, the most common and basic method is Visual Testing (VT) whereby visual examination is conducted to look for cracks etc. in a material. Some prominent methods are listed below:

1. Visual/Optical Testing (VT/OT)
2. Penetrant Testing (PT)
3. Magnetic Particle Testing (MT)
4. Ultrasonic Testing (UT)
5. Guided Wave Ultrasonic Testing / Long Range Ultrasonic Testing (GWUT / LRUT)
6. Eddy Current Testing (ET)

7. Radiographic Testing (RT)
8. Acoustic Emission Testing (AE)
9. Infrared/Thermal Testing (IRT)
10. Remote Field Testing (RFT)

### ***1.1.2 Guided Wave Ultrasonic Testing***

Ultrasonic Testing (UT) is one of the oldest and widely known methods for detecting, localizing and characterization of flaws embedded deep in different structures. It uses bulk waves that pass through the specimen, as depicted in Figure 1-2. The irregularities cause reflections or loss of energy, which is detected. Similarly, but conversely, Guided Wave Ultrasonic Testing (GWUT) uses guided surface waves, which travel across the specimen, as depicted in Figure 1-2. These guided waves interact with any irregularities, causing reflections or loss of energy, which leads to flaw detection. However, guided waves allow in-situ NDT of various structures comprising sheet-like components such as plates, pipes, storage tanks, or vehicle skins including aircrafts, ships and other vessels [6]. GWUT is being utilized in modern petroleum industry and in many other sectors for pipeline inspection. Aerospace, maritime, or civil structures as well as rail networks are also few emerging GWUT applications.

GWUT predominantly uses *Lamb waves*, a type of guided surface waves, to detect and localize cracks; Lamb waves are usually excited at ultrasonic frequencies within the specimen, as stress waves. This can be achieved through various methods like magnetostriction or surface-pinching. Thus, many transducers can be utilized to create in-plane strains required for guided waves. However, PZT wafers are inexpensive, light, and robust as compared to other transducers, and a preferred choice for majority of GWUT based SHM applications [7]. After successful generation, stable propagation of guided waves requires a typical structural boundary

or *waveguide*. That is, the thickness of the specimen should be far less than the excited wave's wavelength [6]. Figure 1-2 depicts a comparison of lamb waves with bulk waves used in conventional UT.

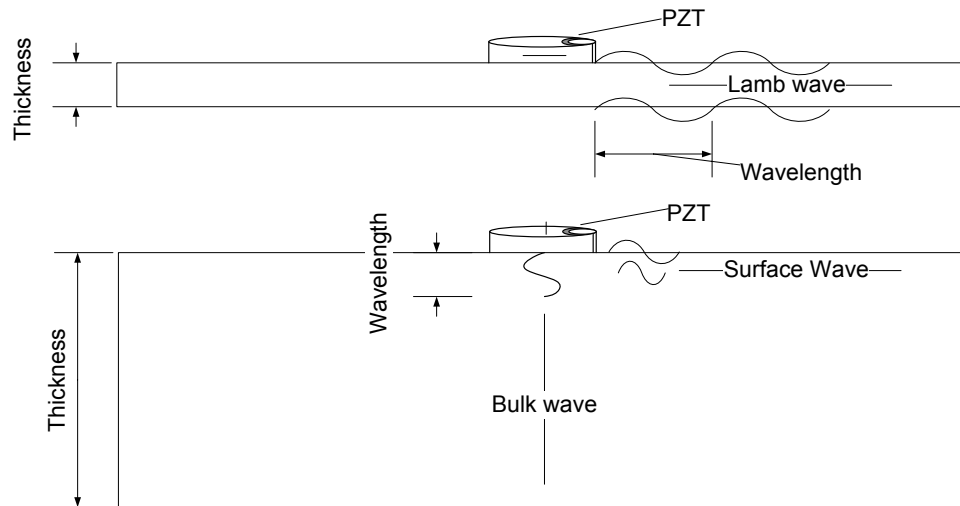


Figure 1-2: Bulk waves for UT versus lamb waves for GWUT

### Pros and Cons

GWUT has many unique advantages over other methods:

4. GWUT enables long range inspection – a potential to achieve hundreds of meters of inspection range.
5. GWUT enables inspection of limited access areas, such as:
  - a. Insulated lines
  - b. Elevated locations
  - c. Buried pipelines
6. GWUT is performed offline, and its signals can be easily recorded for fully automated detection and localization.
7. GWUT allows inspection of both metallic and non-metallic composites.
8. GWUT detects both surface and sub-surface cracks reliably.

The disadvantages of GWUT are:

1. With GWUT it is difficult to find small pitting defects, until they grow into a hairline crack.
2. For complex geometries, interpretation of signals becomes incomprehensible without detailed Finite Element Modeling (FEM) analysis.
3. GWUT needs good procedure and skills, making the interpretation of signals highly operator dependent.

### Applications and prospects in Pakistan

GWUT has applications in various domains. It has following prospects in Pakistan:

#### *Civil Works and Army*

A large number of bridges are present in Pakistan. There is a history of collapse of bridges of different ages in Pakistan due to natural calamities as well as material / construction failures. Such collapses cause serious damage to transport vehicles. Moreover, risk to precious human lives also exists in such collapses. Furthermore, communication lines cease in case of bridge collapse. Therefore, GWUT can be adopted for testing the integrity of bridges after construction and during service life. Pakistan Army engineering core is responsible for rigging bridges during war. SHM of those steel bridges is also possible through this initiative. Moreover, FWO and NHA are also involved in construction and maintenance of highways, bridges and civil structures.

### *Aerospace Research and SUPARCO*

All rockets / missile systems, spacecrafts or satellite systems, whether military or civil, demand high reliability and precision in all aspects of design. Any such critical system must undergo detailed non-destructive tests, especially for flying models, to meet the tough aerospace constraints. GWUT can be a good candidate for in-situ tests after assembly of flying models, or can be installed as SHM system on prolonged missions, such as geo-stationary spacecrafts.

### *Civil Airlines and Air force*

In the recent past, a number of incidents many of which led to major accidents occurred in Pakistan's Airspace due to inadequate overhauling or operation. Guided Wave Ultrasonic Testing can be employed as an effective NDT technique to detect cracks or other faults in riveted joints etc. that may not be visible with naked eye. Research is also being carried out to extend such techniques to automated SHM that would be built-in onboard the aircraft.

### *Maritime Services and Navy*

GWUT along with SHM can be employed to ship's hull and storage tanks etc. for condition-based maintenance and accurately scheduling overhauls. Ship breaking industry might use it for screening different parts.

### *Pipelines and Rail Tracks*

Guided Wave Ultrasonic Testing is already successfully applied for NDT of pipeline inspection and is also being considered for NDT and SHM of rail tracks. Current projects and

already installed pipeline / rail network in Pakistan can benefit alike from such NDT techniques to improve reliability, safety and reduce extra maintenance costs.

### ***1.1.3 Structural Health Monitoring***

Structural Health Monitoring (SHM) is deployed when an engineering structure is to be monitored continuously, either for change in properties or against growth of defects. It also provides online detection, which enables condition-based maintenance – a type of preventive maintenance. SHM systems can continuously log different parameters and generate indications for out-of-range values, which engineers can further inspect and timely schedule maintenance before critical failure. This is achieved by installing an array of sensors on the structure to be monitored, and then periodically sampling their response. These responses are then processed, usually by comparison to a set of reference measurements, or by feeding a mathematical model, to determine any irregularities. These irregularities may then be classified as defects, flaws, damages or change in environmental/loading/boundary conditions, and then localized to determine their position for either further inspection and/or repair. The defects may also be characterized and logged into database. The databases thus developed can also be used for failure prognosis of the structure, such as to predict the remaining useful life or growth of a defect beyond acceptable limits.

### ***1.1.4 Wireless Sensor Networks***

Wireless Sensor Networks or WSN are spatially distributed networks employed for remote sensing, monitoring or logging of various parameters, depending on the application. A WSN is typically composed of *sensor nodes* or *motes*, also called the ‘WSN platform’; optional *gateway* nodes; and a Base Station (BS). The sensor nodes are meant to measure the desired

physical parameter, optionally process them, and transmit them to BS. The gateway nodes are required to relay data from a usually slow data connection with the sensor nodes to a high bandwidth connection (and extended range, sometimes wired) with the BS. A sensor node typically consists of the desired set of sensors interfaced with a low power microcontroller, a radio transceiver, an on-board antenna, and a low capacity power source. The WSN platform design is desired to be low power, low cost, and robust with enough computing resources, and is envisioned to approach a size to make ‘smart dust’ a reality. Thus, the software used for WSN has to be power efficient and fault-tolerant implementation for automatic network configuration.

## **1.2 Research Objectives**

### ***1.2.1 GWUT based wireless SHM***

As discussed earlier, many of the contemporary techniques for NDT are not suitable or readily applicable for SHM [8]. However, GWUT has successfully emerged as an alternative NDT technique, directly applicable to various SHM systems including but not limited to bridges, pipelines, aircrafts, and other vehicles such as in Integrated Vehicle Health Management (IVHM) [7]. Thus, a lot of research is being conducted to design and develop appropriate instrumentation for GWUT based SHM systems. However, wired SHM systems incur heavy installation costs in terms of long running cables, and also require extra maintenance effort for the wiring itself. To overcome these costs, it is often desirable to deploy wireless SHM systems using Wireless Sensor Networks (WSN) [9,10,8]. But wireless SHM systems rely on pre-installed replaceable batteries, which may be complemented by power-harvesting techniques, to transmit or receive signals. Thus, wireless SHM systems particularly their remote instrumentation needs to have extremely low power consumption to avoid starvation out of drained batteries between recharge

cycles. Moreover, the cost and size per node for WSN based SHM system should be kept at minimum to allow practical and feasible large-scale application.

Therefore, the core objective of this research is to foster the knowledge in GWUT based wireless SHM systems, and come-up with an efficient system design for remote sensing in this particular area.

### **1.2.2 Objectives**

Following were the detailed objectives of this research work:

1. First ever generation and detection of guided waves, with bare transducers in Pakistan's academia, after appropriate selection and procurement of transducers, couplant, and test specimen.
2. Signal processing to detect and/or localize cracks via offline processing on PC. The aim shall be to draw conclusions for on-mote processing or wireless SHM.
3. Signal shall be processed on the Remote Station (RS) by hardware / firmware co-design to extract significant statistical parameters/features.
4. The statistical feature(s) of the received signal must be transmitted to the Base Station (BS). This transmission shall be power efficient than current methods.
5. The statistical parameters/features may be transmitted to the BS with appropriate packetization/encoding. A customized packet header may be used considering scalability of the entire system.

### **1.3 Dissertation Outline**

The dissertation has been laid out as follows:



Chapter 2 reviews the literature for relevant research work, highlighting contemporary solutions and their limitations. It also presents the thesis statement of this dissertation.

Chapter 3 covers the detailed theoretical background for GWUT in depth, starting from waves in a plate through testing configurations.

Chapter 4 presents the experiments under taken in this study in detail, resulting designs/codes, and their results.

Chapter 5 defends the thesis by comparing the work with current solutions, states the conclusion, and provides recommendations for future work.

## Chapter 2 Literature Review

---

### 2.1 Relevant Work

Giurgiutiu in [7] covers a pioneering work in this area. The paper has derived expressions for Lamb waves under Piezo-electric Wafer Active Sensors (PWAS) or PZT wafer excitation, which it claims have never published before. The amplitude spectrum derived depends on a  $\sin(\xi a)$  term that causes the response maxima when  $2a$  is odd multiple of half the wavelength and vice-versa, where  $2a$  is the length of PWAS (PZT). Moreover, each Lamb wave mode has its own set of maxima and minima, which means that for different excitation wavelengths, the ratio of strengths of various modes will be different. Further, Lamb waves are generated and propagate in an omni-directional pattern, which is verified experimentally in the study. The study also experiments PZT (PWAS) based excitation of lamb waves with an aircraft panel featuring splice joint and rivets, using the pulse-echo method. It separates the reflection from an EDM emulated crack by the differential signal method: subtracting the received signal from the undamaged received signal. The paper claims to have developed an Embedded Ultrasonic Structural Radar (EUSR) using phased array of PZT (PWAS) transducers for thin wall structures by steering Lamb waves generated from a particular position. It also claims to have identified a PZT (PWAS) self-test method: the dis-bonded transducer shows strong self-resonance when impedance spectrum is observed, and shows no structural resonances and vice-versa.

Michaels and Michaels in [11] presents one fundamental signal processing approach for GWUT signals. The study uses a differential feature based approach to detect changes in the measured signal and classify them as 'structural' or 'environmental'. This helps making the

GWUT technique more robust, or alternatively, applicable to unsuitable circumstances. The study used a 2"x6"x3/16" 6061 aluminum plate which is usually not suitable for guided waves because of the boundary reflections. The transducer used is longitudinally polarized, 2.25 MHz PZT disk, with 12.5mm dia. An Ultrasonic pulser receiver (Panametrics 5072PR) is used with a sampling rate of 12.5 MHz and 8 bit resolution. The environmental changes experimented are as follows: temperature variations from 9° to 38° C, non-uniform wetting, and different placements of oil coupled Aluminum block. The structural changes experimented are as follows: Hole 1: 1.98mm to 6.35mm dia., and Hole 2: 1.98mm to 6.35mm dia. The paper reports first arrivals of longitudinal wave, shear wave, and Raleigh wave; and that there were "no obvious" distinguishable characteristics either in time or frequency domain for received signals to adequately classify environmental or structural changes. The study measures the energy of the difference between the received signal and a reference signal, and compares this energy with a threshold to detect a change. All other features considered were of differential nature, i.e. relative to the respective characteristics of the reference signal. Some interesting and prominent features are as follows: relative energy, relative center of energy in time domain, relative curve length, energy of difference between normalized envelopes, 1<sup>st</sup>/2<sup>nd</sup>/3<sup>rd</sup> moments of absolute value of difference between normalized envelopes, slope and error of local time shift versus time determined by Short Time Cross Correlation (STXC), Normalized STXC peak at T=910usec (very late in time domain).

## **2.2 Contemporary solutions for GWUT based SHM**

Lynch and Loh in [2] present a summary review paper for the application of wireless sensor platforms in SHM. It covers nearly all relevant designs in academia as well as commercial domain from 1998 to 2005. It separately presents 'active platforms' which also contain an

actuator circuit. By a glimpse, it appears that the lowest power in the comparison is consumed by the Sazanov et al. (2004) TI MSP 430 platform (similar to TelosB). Note that the paper covers different types of SHM techniques, most of which sense vibration, temperature and other low frequency data of the order of few kilohertz. That is, it does not distinguish designs for guided wave ultrasonic testing methods. High frequency signals of the order of hundreds of kilohertz involved in GWUT-SHM prohibit the direct use of low-power embedded platforms. Thus, only a few systems have been built for wireless GWUT-SHM recently [12,8,13]. These researchers have to use high sampling rates and computing power, and hence, resulted in designs with high power consumption. Dib et al. in [13] designed a system using only IRIS mote for low power consumption, with a sampling frequency of 273 kps, but on the expense of reduced excitation frequency (75 kHz). Whereas, only one team in [8] was able to reduce transmission data volume as discussed below. The lower the data volume, the lower time the wireless transmission will take place, for a given data rate. Thus, lowering the data volumes also decreases power consumption significantly.

Zhao et al. in [12] presented two approaches of wireless GWUT-SHM for an aircraft wing. In first approach, the study used direct coupling of monopole on-board antenna with piezoelectric Poly-Vinylidene-Fluoride (PVDF) comb transducers for excitation and sensing. The monopole antenna is also capacitively coupled to transmitting and receiving antennas. In second approach, an embedded structural health monitoring system is designed and developed. It is also wirelessly powered, using a horn antenna transmitter and a rectenna (rectifier-antenna) patch array. The power transfer is discussed in detail in the paper. The design of converter for ultrasonic pulser is based on half-bridge resonant inverter circuit, whose output is isolated via transformer. A resistance in parallel to PZT is also installed for fast operation. The study has

compared its embedded ultrasonic device called ‘Umote’ with two other platforms, and has claimed the on-board pulser and multiplexers as a set of novel features. However, the sensing circuit comprises of an 8x8 channel Analog multiplexer/de-multiplexer based on mechanical relays, external 8-bit ADC of 10 Msps with programmable-gain amplifier, a mixed-signal ISP flash microcontroller, and separate wireless modules. The signal sensed from the transducer is sampled directly, and wirelessly transferred to PC for further processing. Hence, the components in addition to the wireless modules simply add to design complexity and power consumption, in trade of handling a complex signal. Moreover, since the signal is transmitted without any processing, there is no reduction in data volume.

Pertsch et al. in [8] introduced a Hilbert-transform based envelope detection algorithm for estimating the peak values of the sensed signal correctly. This also led to great reduction in data volume, because now only the envelope needs to be transmitted instead of the complete signal sampled at much higher rate. The study used a pitch-catch method to detect flaws in a steel specimen using Rayleigh waves, generated by ultrasonic wedge transducer. The prototype designed in the work is based on a TI eZdsp™ F28335 evaluation board, which contains a powerful Digital Signal Processor (DSP) with on-chip DMA, ADC, PWM module, and serial interfaces. This platform connects with a signal conditioning board for sensing, an output amplification board for excitation, and wireless transceiver for wireless communication. However, following components are used in series to form the signal conditioning circuit: a passive clipping circuit, a passive HPF, a non-inverting amplifier with offset correction, and a 3rd order active Butterworth low-pass filter whose output is fed to the on-chip 12-bit ADC, running at 8.3334 Msps. Then the Hilbert transform is taken on-board, and signal is transmitted using the wireless transceivers. Finally, the study claims to save battery power and time by

wireless transmission of envelopes instead of original signal; and presents the prototype as a low-cost solution, emphasizing the use of the amplitude of the received signal as the damage signature. Nevertheless, data volume was reduced, but on the cost of greater power consumption in the evaluation board in addition to signal conditioning board. Moreover, the high excitation frequency demanded very high sampling rates. Though sampling was done roughly at eight times the excitation frequency, missing samples forced the use of Hilbert transform.

The study has also supported embedded ultrasonic testing with a reference experiment (also discussed in detail) to find amplitude transmission coefficients for notches. The maximum deviation of amplitude transmission coefficients for notches using embedded ultrasonic testing is less than 10%.

### **2.3 Limitations of current solutions**

Current solutions use high speed ADCs that are expensive and increase the power consumption of the entire system both directly and indirectly. For most ADCs the power consumption is proportional to sampling rate. Further, large number of samples increase the active wireless transmission time for a given data rate and thus power consumed by the system.

Some researchers attempted reduction of data volume transmitted wirelessly but ended in large powers wasted by powerful microprocessors for implementing complex signal processing algorithms. Moreover, the use of additional expensive components apart from the wireless modules at each node increased the overall cost of the system, making large-scale application infeasible.

## **2.4 Problem statement – Thesis**

To enable low-power sensing in wireless GWUT-SHM, one has to overcome conventional constraints presented. This work presents a novel approach for low-power wireless GWUT-SHM by a system design which reduces the sampling rate requirement and transmission data volume, thereby reducing the power consumption of the complete system.

## Chapter 3 Guided Wave Ultrasonic Testing Theory

---

### 3.1 Waves

Any set of periodical vibrations or oscillations that travel along a matter, usually resulting in transfer of energy, is called a 'mechanical wave'. An excitation or disturbance in a matter causes the generation of mechanical waves that distribute the injected energy from the excitation point throughout the medium, depending upon the type of wave. In solids, different types of waves originate owing to various degrees of freedom – number of possible directions of vibrations for molecules. A wave mode or mode of vibration is a characteristic oscillatory pattern capable of stable propagation, also characterized by its modal frequency. There major types of mechanical waves depending upon the particle motion are as follows:

1. Longitudinal waves: where direction of particle motion is along the direction of wave propagation, for example, Compressional waves.
2. Transverse waves: where direction of particle motion is perpendicular to the direction of wave propagation, for example, Flexural waves.
3. Surface waves: where particle oscillates in an elliptic orbit motion resulting in combined longitudinal and transverse motions.
4. Plate waves: are surface waves generated at both sides of a plate, not thicker than a few wavelengths.



### 3.1.1 Lamb waves and Guided waves

Lamb waves are basically plate waves, introduced by Sir Horace Lamb in his famous article “On waves in an elastic plate” in 1917 [14]. In this article, he derived the solutions to the wave equation for waves propagating in thin infinite plates. But the numerical solutions of these equations came with the advent of modern computing era in 1990s. Later, for practical application in finite mediums, it came out that such waves can sustain if certain boundary conditions are met, that is, if the waves are *guided*. Mathematically, the expressions governing the motion of lamb waves are as follows:

$$\xi = A_x f_x(z) e^{i(\omega t - kx)} \quad (1)$$

$$\zeta = A_z f_z(z) e^{i(\omega t - kx)} \quad (2)$$

Where,  $\xi$  and  $\zeta$  are the displacements along x-axis and z-axis respectively. Note that these displacements are only a sinusoidal function of time, x-axis, or z-axis, but are independent of y-axis. Thus, the lamb waves are 2-dimensional, that is, the particles vibrate on a plane formed by the axis of wave propagation and it's normal. This means that there is no displacement along the y direction. However, many such waves propagate in all directions just like light waves coming from a point source, or more appropriately, like ripples that form when a pebble is thrown into water.

By applying the boundary conditions of a free surface plate on (1) and (2), that is, zero stress at the surfaces ( $z = \pm d/2$ ), the characteristic equations are derived as under:

$$\frac{\tan\left(\frac{\beta d}{2}\right)}{\tan\left(\frac{\alpha d}{2}\right)} = \frac{-4\alpha\beta k^2}{(k^2 - \beta^2)^2} \quad (3)$$

$$\frac{\tan\left(\frac{\beta d}{2}\right)}{\tan\left(\frac{\alpha d}{2}\right)} = \frac{(k^2 - \beta^2)^2}{-4\alpha\beta k^2} \quad (4)$$

Where,

$$\alpha^2 = \frac{\omega^2}{c_l^2} - k^2, \text{ and } \beta^2 = \frac{\omega^2}{c_t^2} - k^2$$

$c_l$ ,  $c_t$ ,  $\omega$ ,  $k$ , and  $d$  are respectively: longitudinal velocity, transverse velocity, angular frequency, wave number, and plate thickness. (3) and (4) represent the *symmetric* and *anti-symmetric* modes as discussed next. The term *guided* thus refers to the wave propagating in a finite waveguide, which satisfies the boundary conditions. However, for a structural component to be a waveguide requires its thickness to be comparably small than the wavelength of the wave [6]. Thus, example waveguides are plates, pipes, rods, rails etc.

### Modes

Lamb waves have predominantly two families of modes: symmetric and anti-symmetric. Symmetric modes are also called Extensional modes because they effectively stretch and compress the plate along mid-plane, where  $z = 0$ , and their particle displacement along the direction of wave propagation is larger than along the normal, which is why they are also referred to as the Longitudinal modes. Anti-symmetric modes are also called Flexural modes because they effectively bend the plate about the mid-plane, and their particle displacement along the direction of wave propagation is smaller than along the normal, which is why they are also referred to as the Transverse modes. Figure 3-1 depicts propagation of the two mode families for lamb waves.

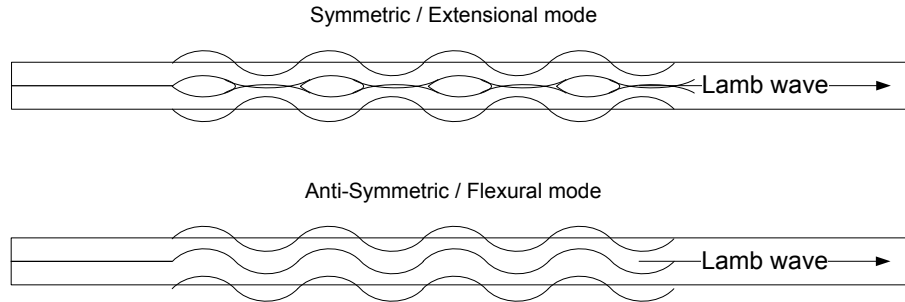


**Figure 3-1: Lamb wave mode families**

Zero order symmetric  $S_0$  or anti-symmetric  $A_0$  modes are present for entire spectrum of lamb waves. Higher order symmetric or anti-symmetric modes excite at each resonant frequency of the plate and sustain indefinitely.

### Dispersion

Normally, speed of a wave is given by its frequency wavelength product, and it's unique. However, lack of certain degrees of freedom in a material can cause the frequency to be a function of the wavelength or wave number. Consequently, a propagating wave splits into its frequency components, as it passes through a dispersive medium. Lamb waves (waves in plate) are also dispersive in nature. The relation of phase velocity and group velocity with the excitation frequency is inherent in (3) and (4), and is conveniently represented by the dispersion curves as a function of frequency thickness product. Figure 3-2 and Figure 3-3 show the dispersion curves for Al 6061, transducer (PZT) length of 10 mm, plate thickness of 2 mm, obtained by Wavescope v2.5 (from LAMSS, USC) for phase and group velocity respectively.

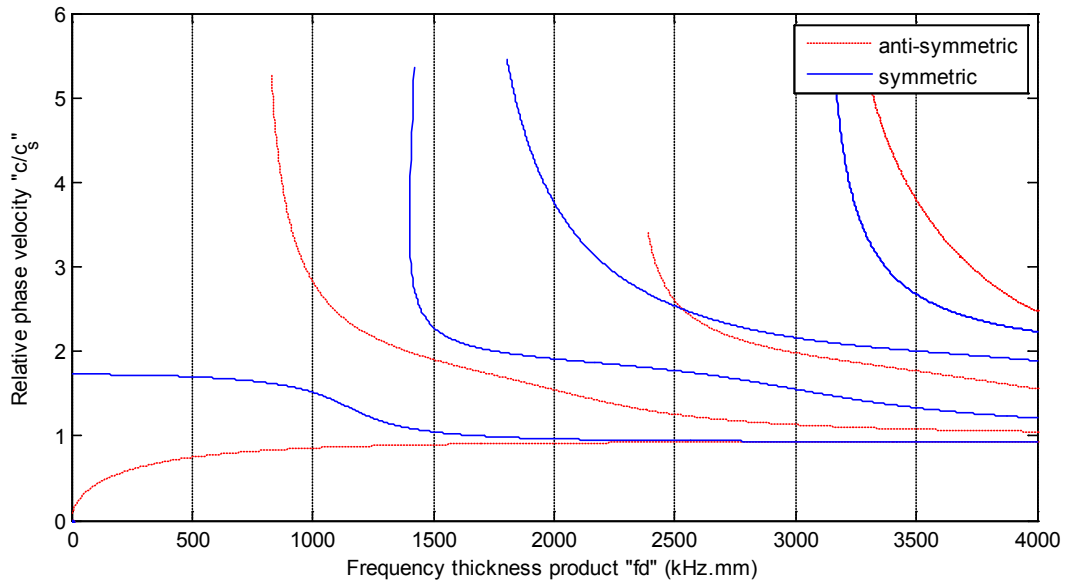


Figure 3-2: Lamb wave phase velocity dispersion curve for Al6061, 2a=10mm, 2d=2mm

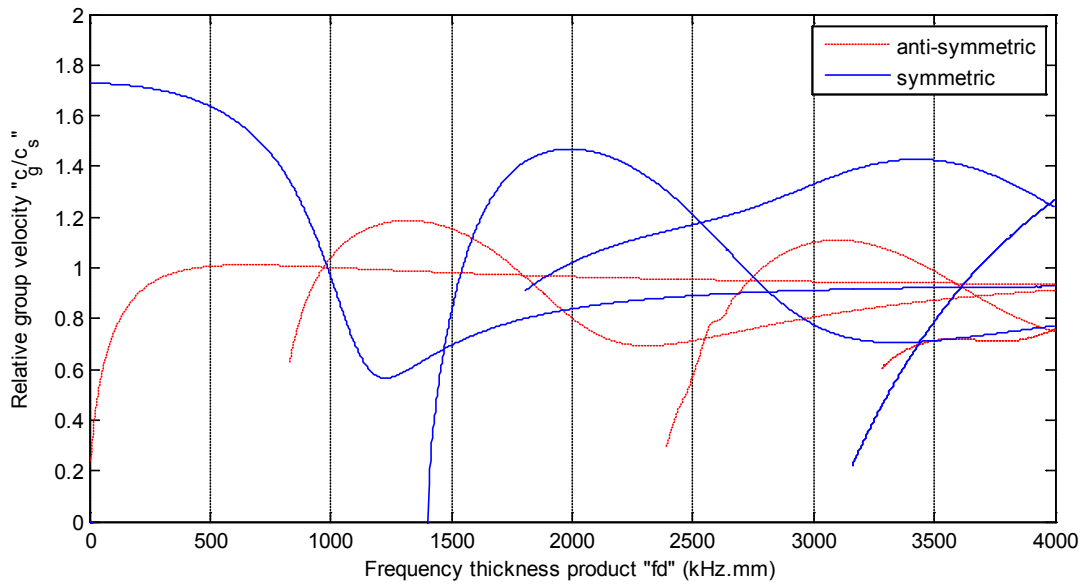


Figure 3-3: Lamb wave group velocity dispersion curve for Al6061, 2a=10mm, 2d=2mm

It's important to note here that the curves are for velocities relative to shear wave velocity for Al6061 (3099.6 m/s). Further, as the frequency-thickness product is increased, new lamb wave modes are excited and sustain indefinitely. Therefore, to work only with the primary modes i.e.  $A_0$  and  $S_0$ , one needs to keep the frequency-thickness product less than that of the second

mode excitation. Moreover, the group velocity is the velocity of the waveform or wave-envelope, whereas the phase velocity is the velocity of a particular phase-component. Therefore, the group velocity curves are of practical significance, because group velocity is what we observe in an experiment.

Depending upon various parameters, a wave mode can be dispersive or non-dispersive. Dispersive modes tend to decay over time, because different components travelling at different speeds cause the overall waveform to decrease in amplitude and stretch in time domain [6]. However, non-dispersive modes exhibit consistent amplitude and pulse duration. Therefore, lamb waves can be used for in-situ testing of structural components.

### 3.2 Generating Guided waves

Guided waves can be generated primarily by two mechanisms: Total Internal Reflection (TIR) or Surface Pinching. In the former, the waves are incident at a specific angle calculated using Snell's law to cause internal reflections, instigating guided waves [6], as depicted by Figure 3-4. This method requires bulky transducers, and is usually suitable for lab testing only. Lamb waves thus generated are extremely sensitive to the angle of incidence and couplant used.

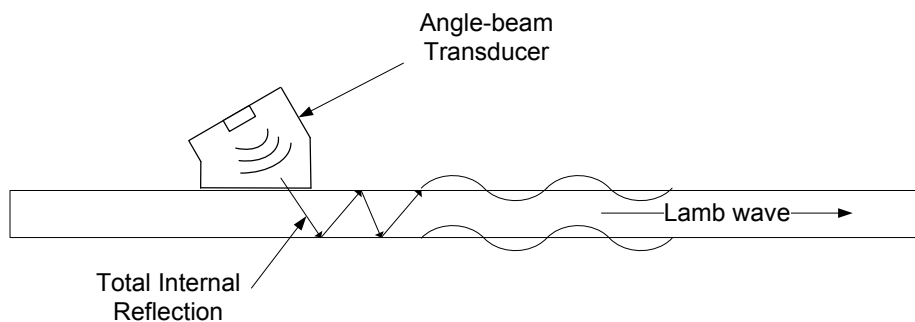


Figure 3-4: Lamb wave generation using Snell's law

The other method requires pinching the surface to cause elliptic motion of molecules beneath the surface, producing lamb waves, as depicted in Figure 3-5. This requires the

transducer to be strongly coupled to the surface or through a proper couplant. Since these types of transducers are light and can be mounted permanently, they are better choice for SHM.

References [7,15,16] discuss this method in detail.

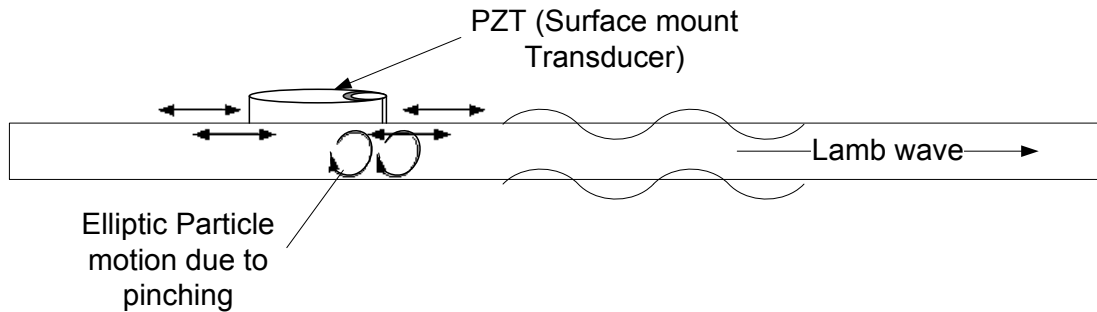


Figure 3-5: Lamb wave generation through surface pinching

### 3.2.1 Transducers used for exciting Guided waves

Following transducers can be used for generating guided lamb waves:

1. Electro-Magnetic Acoustic Transducers (EMAT): operate by electromagnetic induction into specimen, producing eddy currents. These eddy currents experience Lorentz force in the presence of magnetic field, and consequent interaction of electrons with molecules produces acoustic waves. This method produces low intensity waves, which are difficult to sense, and is now used for specialized applications requiring non-contact or couplant-less method.
2. Piezoelectric transducers (PZT/PWAS): can generate guided waves using either TIR or surface pinching. They are very light, robust, and cheap, but require a suitable couplant to transfer their vibrations.
3. Magnetostrictive transducers: are applicable to only ferromagnetic materials, and operate through magnetostriction.

### ***3.2.2 Generating Guided waves using piezoelectric transducers***

Piezoelectric effect was first discovered in Quartz by Curie brothers. However, later many compounds were studied for piezoelectricity, and Lead Zirconate Titanate (PZT,  $\text{PbZr}_{0.52}\text{Ti}_{0.48}\text{O}_3$ ) became the most common piezoelectric transducer. A raw crystal is spliced at specific angles to produce a PZT wafer with specific properties. PZT wafers are available in different shapes, sizes and vibration modes. The three major modes of vibration for piezoelectric transducers are:

1. Thickness mode: Plate or disk that vibrates along its thickness.
2. Shear mode: Plate or disk that vibrates by shear deformation.
3. Radial mode: Disk that vibrates radially outwards.

Radial mode PZT transducers are used to generate guided lamb waves by surface pinching, as shown in Figure 3-5. Many different PZT wafers are available from various manufacturers around the world. Because a slight variation in manufacturing process changes any of the several piezoelectric properties of the wafer, some standard classes of PZT wafers are defined by the industry. PZT-5A and PZT-5J have the most modest properties for generating lamb waves.

Of different properties, the most important practical property turns out to be the resonant frequency of the PZT wafer. A typical PZT material has many resonances, but there are always two prime ones which are significant: series resonant frequency and parallel resonant frequency. The series resonant frequency ' $f_s$ ' or simply resonance frequency ' $f_r$ ' is the lower one, and offers minimum impedance to the source. This is the natural resonant frequency of the material and also denoted by ' $f_m$ '. The parallel resonant frequency ' $f_p$ ' or anti-resonance frequency ' $f_a$ ' is the higher one, and offers maximum impedance to the source. This is parasitic resonant frequency

due to the parallel electrodes and also denoted by ' $f_n$ '. Resonant frequency is important, because we get suitable transduction efficiency only at resonance. This makes another parameter 'Q-factor' important. The higher the Q-factor, the larger the transduction, but narrower is the resonant bandwidth, which is a significant trade-off. Another practical parameter is the Curie temperature: the temperature above which the wafer loses its piezoelectric properties permanently. This requires temperature controlled soldering of contact wires to the PZT wafer. Obviously, the Curie temperature must be high enough to allow soldering of contact wires. Furthermore, the PZT wafers need to be placed and electrically connected in a specific manner as depicted in Figure 3-6; the plate should be at the reference potential, otherwise, the signal will be corrupted.



Figure 3-6: Correct electrical alignment for PZT wafers

### 3.2.3 Role of couplant

Practically, PZT wafers can't be clamped with the specimen without air-gaps easily. Therefore, a *couplant* is needed to match the acoustic impedance of the transducer with the specimen under test. This minimizes the loss of energy at the interface by displacing the air. A couplant can be liquid, solid or semi-solid. For conventional UT, many couplants can be used, such as glycerin, silica-gel, honey, grease etc. However, liquids do not allow transverse or shear waves through them, which makes liquid couplants poor contender for lamb waves. Therefore, semi-solids like silica-gel or cured-solids like cyanoacrylate are good couplants for lamb wave generation, because surface-pinching is a shear-deformation process.



### 3.3 Guided Wave Ultrasonic Testing

Guided waves are being used for flaw and irregularity detection in structures. Any flaw in form of void or crack interacts directly with the guided wave propagation, causing reflections, loss of energy, or mode conversion. These changes can be detected by either in-situ or dynamic sensing. There is more than one method to conduct GWUT, as discussed below.

#### 3.3.1 Configuration modes for GWUT

GWUT systems can be primarily of either pitch-catch configuration [13,8] or pulse-echo configuration [7,12]. In pitch-catch configuration, as shown in Figure 3-7, one transducer acts as an actuator and generates guided waves in the specimen. Another transducer senses the waves directly after propagating through a distance. Any fault in between is detected as a change in the received signal strength.

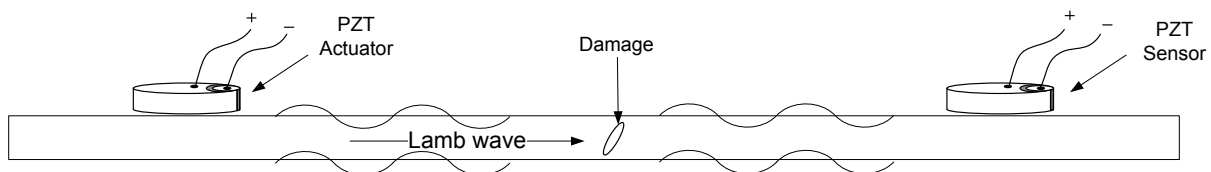


Figure 3-7: Pitch-catch configuration

In pulse-echo configuration, as shown in Figure 3-8, a single transducer or a pair is used to generate the guided wave pulses into the medium, and sense the echoes in-situ over time. This method is usually more suitable for SHM. Echoes reflected from the structural boundaries can be saved as reference, allowing change detection by comparison.

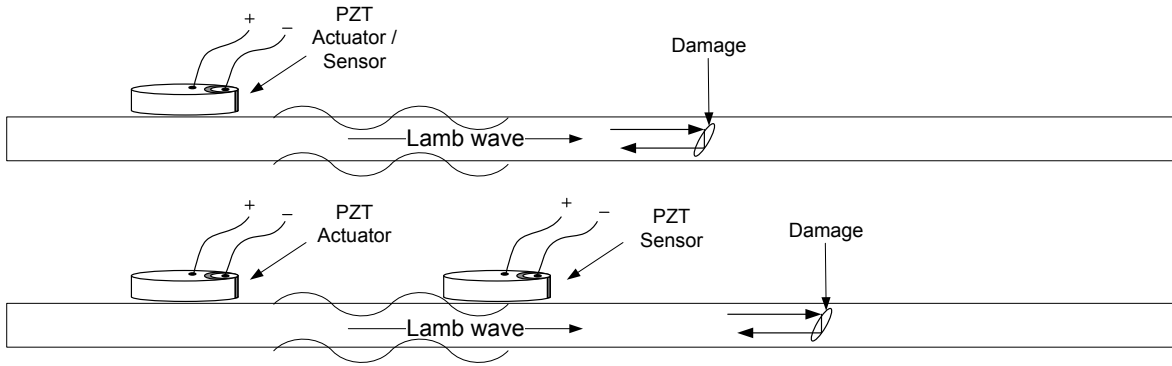


Figure 3-8: Pulse-echo configuration: with single transducer (shown atop), with pair (bottom)

### 3.3.2 Localization using GWUT

To localize cracks on a two-dimensional plane, an array of transducers is needed. The transducers in these arrays can be placed at specific geometric points, and excited in a particular fashion to localize flaw using triangulation or other navigational / imaging techniques [17,12]. In other approach, transducers can be placed in small grid or cut in particular shapes (such as combs) to excite a straight beam of guided waves in a particular direction (controllable by excitation pattern) rather generating spherical wave-fronts [5]. Distance of the flaw from the transducer is usually determined by time of arrival of reflected wave-fronts, given the speed of the wave mode in that material.

## Chapter 4 Experiments

---

### 4.1 Selection of specimen, transducers and couplant

The test specimen for all experiments was an Aluminum Alloy Al6061-T6, having dimensions: 1.219 m x 0.914 m x 0.002 m (4' x 3' x 0.079"). The alloy is 95.85%–98.56% Aluminum; containing silicon, magnesium, and traces of other metals. It is heat treated and artificially aged for robustness. It was selected because of its wide applications in aerospace as well as commercial sectors, such as wings, fuselages, rotor skins, space-craft panels, yachts, ship building, SCUBA tanks, bicycle frames, heat exchangers, metallic bridges, boiler tanks etc.

For initial experimentation, radial mode PZT wafer disks of PZT-5J material from STEMiNC (Steiner & Martins, Inc. USA) were used (part# SMD07T03R411). They had a radial mode resonant frequency of 300 kHz, with dimensions: 7 mm (dia) x 0.3 mm (thickness). Later on, radial mode PZT wafer disks of PZT-5A equivalent material (P-33) from UCE (Ultrasonic Co. Ltd., China) were used. They had a radial mode resonant frequency of 200 kHz, with dimensions: 10 mm (dia) x 1 mm (thickness). These PZTs are shown in Figure 4-1 below. In both cases, the frequency thickness product was kept below 800 kHz·mm, in order to avoid excitation of secondary lamb wave modes.



Figure 4-1: PZT-5A equivalent (P33) transducers (unused, + sign indicates positive electrode)

Though cure-solids are good couplants for GWUT, silica-gel was used as semi-solid couplant, because the former are usually permanent adhesives. Glycerin and honey were also tested, which did not produce satisfactory results. The silica-gel used was commercially available from local medical market.

## 4.2 Experimental Setup

### 4.2.1 Excitation

Many researchers have used square or sine wave bursts to excite the transducers [12,5,8]. But due to dispersion and consequent shape distortion, the received signal loses the actual envelope of the signal containing steep transitions. Therefore, the excitation signal was needed to have the group delay as small as possible. Thus, Gaussian pulse was chosen, which offers the best trade-off of steep transitions and group delay. This way, the shape distortion due to group delay will have minimum possible effect on the results. A Gaussian pulse takes the form of a Gaussian function, represented by:

$$f(t) = A e^{-\frac{1}{2} \left( \frac{t-t_m}{t_0} \right)^2} \quad (5)$$

Where A is the amplitude of the signal,  $t_m$  is the peak time, and  $t_0$  is the time of inflection.

Further, to convert maximum (electrical) signal energy into mechanical domain, the Gaussian pulse was amplitude modulated over a sinusoidal carrier whose frequency matched the resonant frequency of the PZT wafer. Hence, a modulated Gaussian pulse was used for excitation of the PZT wafer disk as in [16]. It was generated by using an Arbitrary Function Generator (AFG), the GW-Instek's AFG-2005. The excitation signal is as shown in Figure 4-2, with normalized amplitude. The pulse was repeated by the AFG, at a Pulse Repetition Frequency

(PRF) of 4.884 kHz. The Gaussian parameters were mean ( $t_m$ ) =  $1.419 \times 10^{-5}$  s and variance ( $t_o^2$ ) =  $2.187 \times 10^{-11}$  s<sup>2</sup>, for achieving a fractional bandwidth of 0.4 with reference level of -40dB.

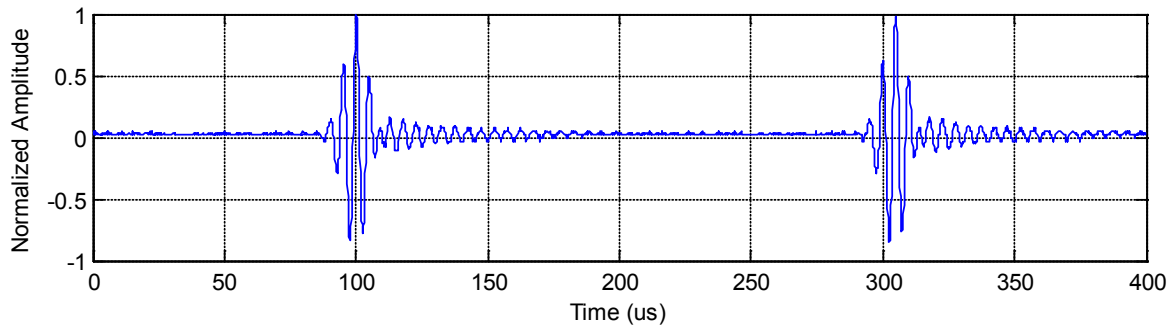


Figure 4-2: Modulated Gaussian pulse as the excitation signal

### 4.2.2 Positioning

To keep things simple, two transducers were used for this experiment. One transducer acted as an actuator that was excited by the AFG and coupled with the specimen, while other transducer acted as a sensor that generated the response / received signal and was also coupled with the specimen. The positioning of these transducers on the specimen is depicted in Figure 4-3. To emulate a crack, two similar sheets of the specimen were used. One was kept unworked, while the other was engraved to form a notch, 2 cm in width and approximately 1 mm deep. The sensor was first connected with the oscilloscope to analyze the generated response / received signal. Later, as discussed in following sections, the sensor was connected directly with the Signal Conditioning Circuit (SCC) for further processing and wireless transmission.

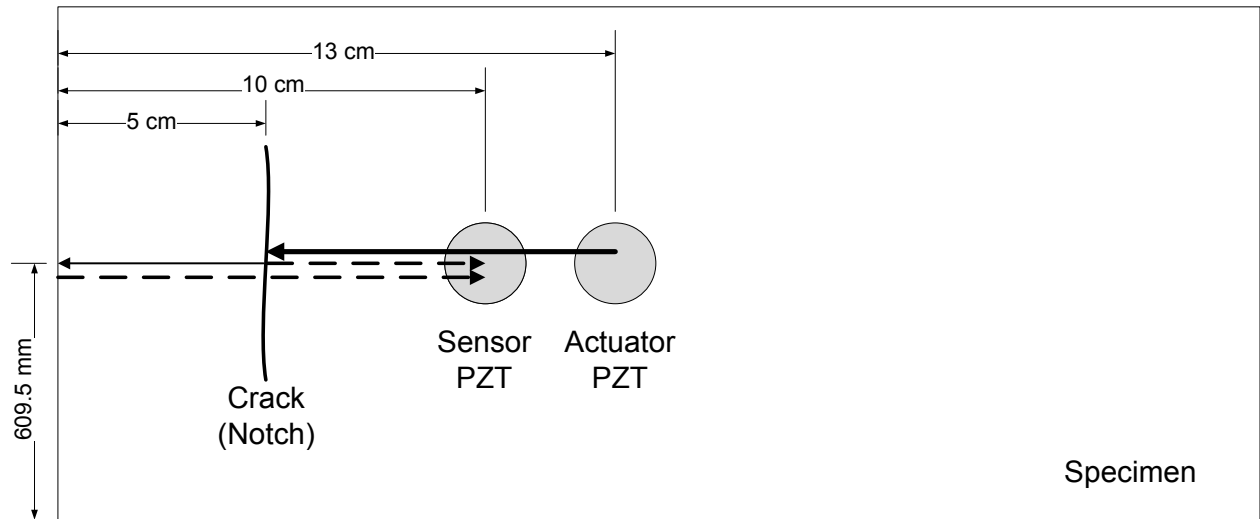
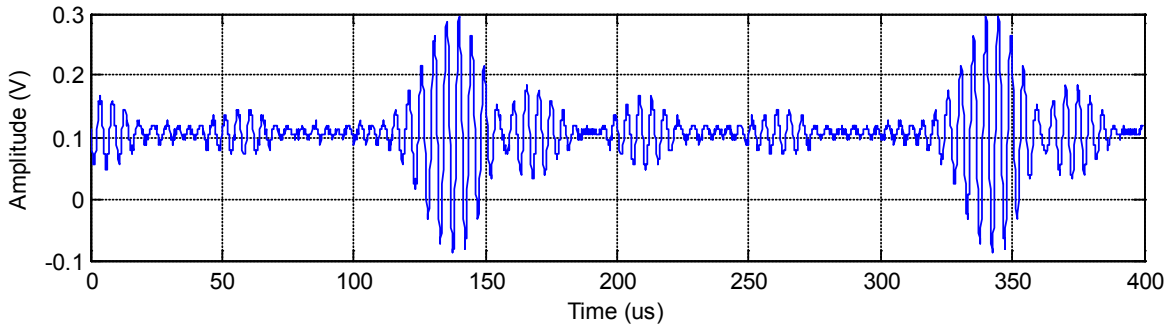


Figure 4-3: Position of transducers on the specimen, top view (not to scale)

### 4.2.3 Methodology

This experiment follows the pulse-echo configuration, as depicted in Figure 3-8, and with a pair of transducers, as discussed earlier. Now, when the actuator PZT shown in Figure 4-3 will be excited, lamb waves will be generated beneath the transducer which will travel omnidirectionally [7]. The wave front of the Gaussian pulse thus formed will reach the sensor PZT first, causing it to generate a corresponding response. Then, the pulse wave will be reflected back from the boundary, and reach the sensor PZT a second time causing it to generate a second response. In presence of the emulated crack, after passing the sensor PZT for the first time, a part of the pulse wave will be reflected back, while the rest of the wave energy will pass the crack to get reflected from the boundary. Thus, the received signal shall be significantly altered in presence of an echo from the crack and a heavily attenuated echo from the boundary. This change in received signal should allow flaw detection. Figure 4-4 and Figure 4-5 show the signals received without the notch, and with the notch respectively.



**Figure 4-4: Received signal from sensor PZT without crack**

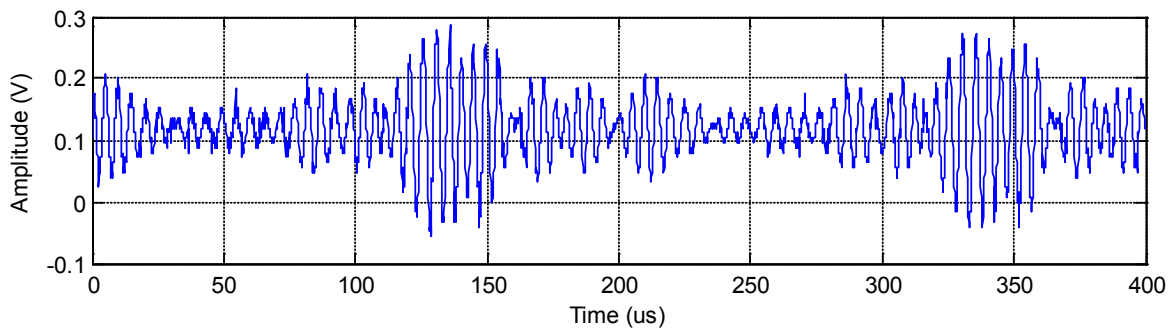


**Figure 4-5: Received signal from sensor PZT with crack**

A plain comparison of the signals received, with and without the flaw, reveals that crucial information relating to the damage / flaw is present in amplitude peaks that form the envelope of the signal. Most of the contemporary researchers have analyzed the received signal directly, however, bearing the fact that the excitation signal was *amplitude modulated* Gaussian pulse; the sensed signal can be first *amplitude demodulated* to yield a lower frequency signal. Subsequent sub-sections explain this approach.

### **4.3 Design of Instrumentation Amplifier and Envelope Detector – The Signal Conditioning Circuit**

Figure 4-6 illustrates complete chain of sensing adapted in this design. The Signal Conditioning Circuit (SCC) consists of an instrumentation amplifier as pre-amplifier, an

envelope detector and low pass filter. It senses the envelope of the signal directly and provides it to the on-chip 12-bit ADC of the zigbee mote that runs at 200 kbps. Each block of the SCC is further detailed as follows:

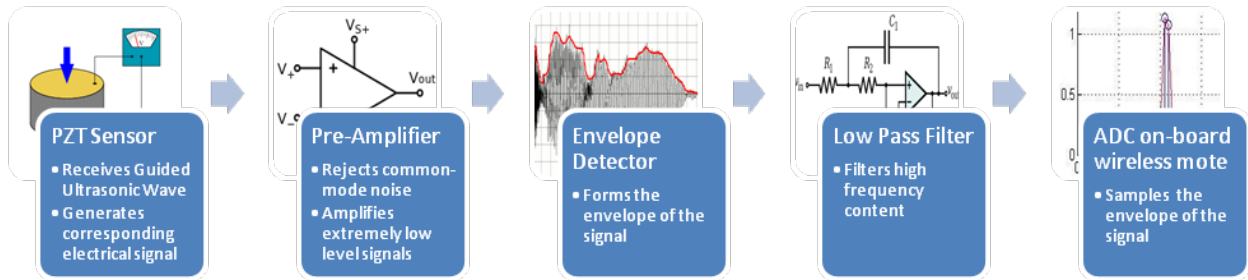


Figure 4-6: Sensing chain for wireless GWUT-SHM

### 4.3.1 Pre-amplifier design

The signals received / sensed off the sensor PZT contain considerable common mode noise, and should be sensed differentially to reject the same. Moreover, the signals are too weak to be sampled directly. The received signals are usually less than 300 mV peak-peak in amplitude. This means pre-amplification is must before further processing. Furthermore, here PZT wafer transducer is the source, which cannot provide significant current. Therefore, the input stage of the pre-amplifier should offer very high differential and common-mode input impedance, to sense the signal efficiently.

Therefore, a low cost, low power Instrumentation Amplifier AD620 has been used for the pre-amplifier circuit. Being an instrumentation amplifier (IA), it senses input signal differentially, with a Common-Mode Rejection Ratio (CMRR) and Power Supply Rejection (PSR) greater than 100 dB for frequencies up to 50 Hz. This precludes the use of passive filters at the input stage, which may deteriorate the signal integrity as in [8]. It also offers very low input bias current of the order of nano-amperes and an input impedance of  $10\text{ G}\Omega \parallel 2\text{ pF}$ .



However, as shown in Figure 4-7, R7 and R8 are installed to lower the circuit's differential input impedance to 2.4 k $\Omega$  for providing a discharge path for the effective capacitance supporting high frequency variations. They also offer balanced differential impedance to provide a ground return path for the input bias current of the IA. Though, ideally, the signal to be sensed should be applied directly to the inputs of IA, but PZT does not provide a ground return, and IA can't work with floating inputs. The circuit for pre-amplifier is shown in Figure 4-7.

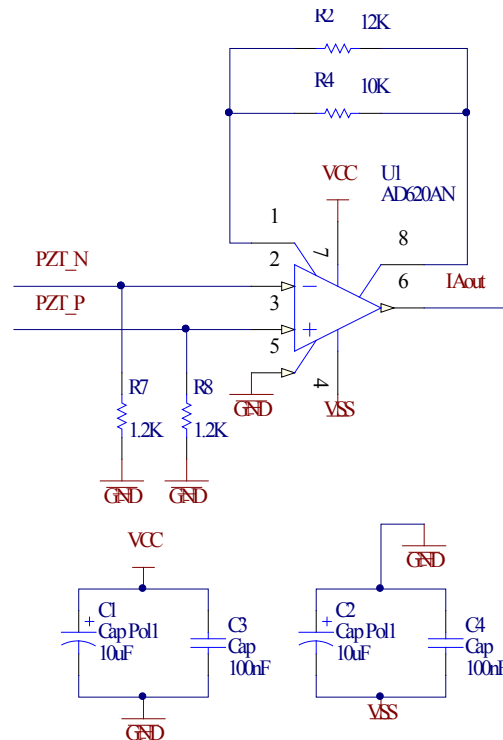


**Figure 4-7: Instrumentation amplifier based pre-amplifier for sensing**

The capacitors connected between the supply rails are the decoupling and bypass capacitors, whose values are recommended in the device datasheet for rejecting external RF interference. The Parallel combination of R2 and R4 is used to obtain 5.45 k $\Omega$  to set the required gain of Instrumentation Amplifier (IA). The gain is set to 10 V/V using the formula from the datasheet:

$$R_G = \frac{49.4 \text{ k}\Omega}{G - 1} \quad (6)$$

This gain is enough for following circuits to function properly. Figure 4-8 shows the input signal amplified by the pre-amplifier.

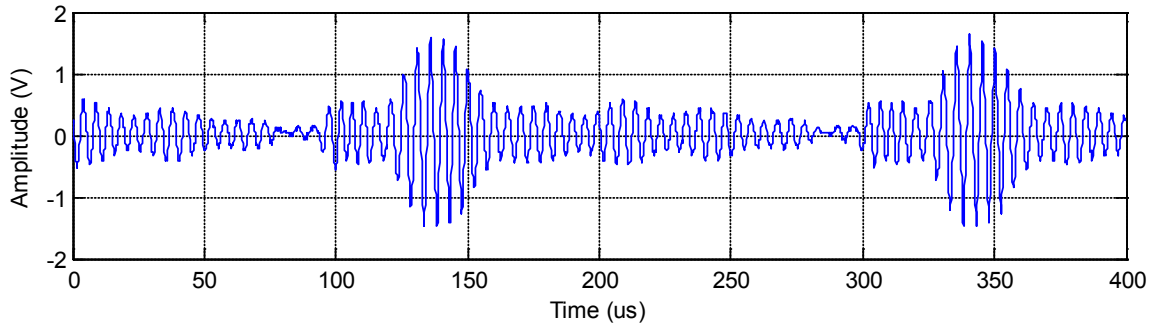
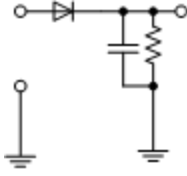


Figure 4-8: Response of pre-amplifier

### 4.3.2 Envelope detector design

Because the information of interest mainly lies in the peak amplitudes or envelope of the signal [8,11], a hardware-based solution is to use an envelope detector for extracting the sensed / received signal's envelope prior to sampling by ADC. This will lower the ADC's sampling rate requirement and subsequently the power consumption, or conversely, allow use of higher excitation frequencies on a given platform.

Moreover, an ideal envelope detector uses a diode capacitor combination, as shown in Figure 4-9, to detect instantaneous peaks arising in a signal. The exact time interval for which the peaks are sought can be adjusted by the RC time constant. But after pre-amplification, the signals of the order of millivolts in this work, will not be more than a few volts and comparable to the forward voltage drop of the diode. This suggests an active precision-rectifier based design implementation.



**Figure 4-9: Ideal envelope detector circuit**

Hence, a precision full-wave rectifier is designed that replaces the diode in the conventional envelope detector circuit, coupled to a low-pass active filter that smoothly follows the envelope of the signal. Compared to half-wave rectification, full-wave rectification turns the negative swings into positive ones effectively doubling the number of peaks within the envelope of the received / sensed signal. This makes low pass-filtering realizable by increasing the gap between envelope signal's and the *carrier* signal's frequency bands. Detailed design is as follows:

### Precision full-wave rectifier design

The full-wave precision rectifier is itself composed of two major circuits, the improved precision rectifier circuit and weighted summer circuit. The improved precision rectifier only performs ideal half-wave rectification overcoming the forward voltage drop and other distortions, resulting in an inverted output. Then the weighted summer circuit adds this output with double weight back to the input signal of the precision rectifier, resulting in a precise full-wave rectified output, as shown in Figure 4-10.

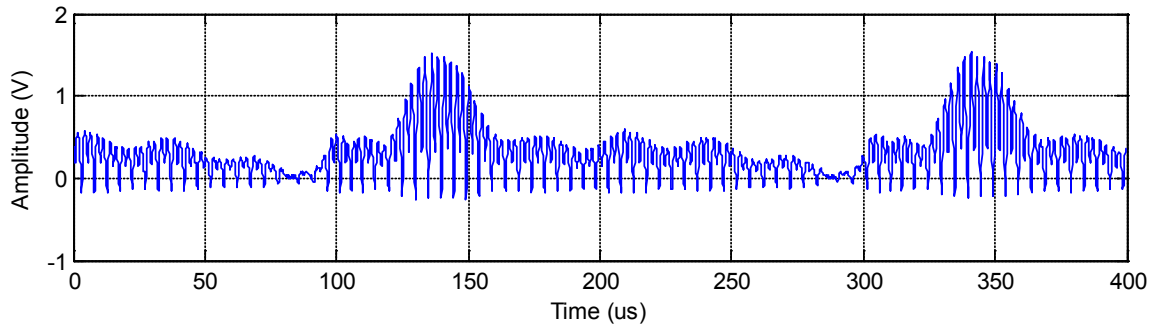


**Figure 4-10: Output of precision rectifier for envelope extraction**

The circuit, shown in Figure 4-11, is based on wideband op-amp TL-082, and two BAT-42<sup>2</sup> small signal schottky diodes. The design implements op-amps in a current feedback configuration to provide better slew-rate performance with minimum distortion. Schottky diodes exhibit very low reverse recovery time, and were used to improve the overall frequency response of the circuit. The 10 kΩ parallel combinations are used to obtain 5 kΩ resistances as per design. All resistances in this circuit should be perfectly matched to let this circuit operate as desired, which is perhaps, the only significant limitation. Though these resistances can be linearly increased to increase input impedance of the circuit, but this has been traded off with desired frequency response of the diodes. The larger the current through schottky diodes, the better frequency response they offer.

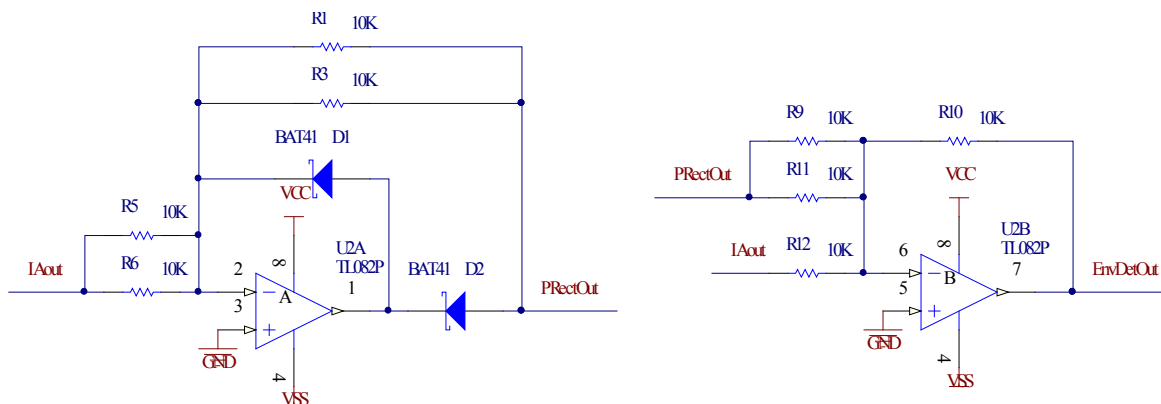


**Figure 4-11: Precision rectifier circuit**

<sup>2</sup> Preferred: BAT 41 can also be used

## Low-pass active filter design

The low-pass active filter circuit low-pass filters the output of the precision full-wave rectifier, but it's essentially designed to follow the superimposed envelope – the signal of interest, which is of Gaussian nature because of the corresponding nature of the excitation signal. Thus, the time-constant of the RC filter should be less than the time period of the highest frequency present in the signal of interest. Alternatively, the maximum rate of change of the superimposed signal should be equal to the slew rate of the active filter circuit, to smoothly follow the superimposed low frequency signal, mathematically expressed in (7). Thus, the superimposed signal is taken as a Gaussian function and its slope is evaluated at its inflection point ( $t_m + t_0$ ), where the rate of change is maximum for a Gaussian function. Moreover, the slew rate for the RC circuit is given by discharge rate of the capacitor, which is highest at the onset of discharge.

$$\max_{t \rightarrow t_m + t_0} \left[ \frac{d}{dt} e^{-\frac{1}{2} \left( \frac{t-t_m}{t_0} \right)^2} \right] = \max_{t \rightarrow 0} \left( \frac{d}{dt} e^{-\frac{t}{RC}} \right) \quad (7)$$

Simplifying the above equation and solving for the RC product, yields a time constant in (8).

$$\tau = RC \approx t_0 e^{-\frac{1}{2}} \quad (8)$$

The time constant came out to be of the order of microseconds; fine tuned to  $5.6 \times 10^{-6}$  s. Figure 4-12 shows the circuit diagram and Figure 4-13 shows the final output of SCC, which is sampled directly by the ADC of the wireless zigbee mote.

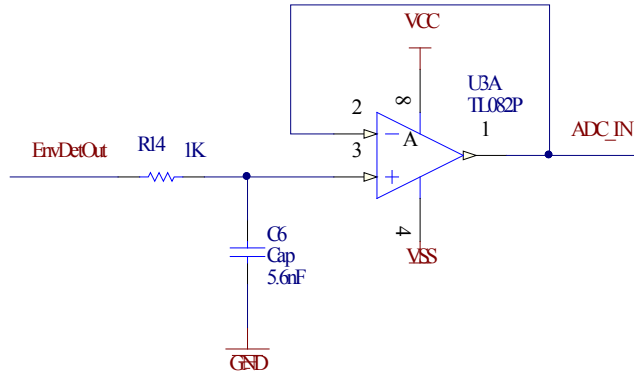


**Figure 4-12: Low pass active filter circuit for envelope detector**

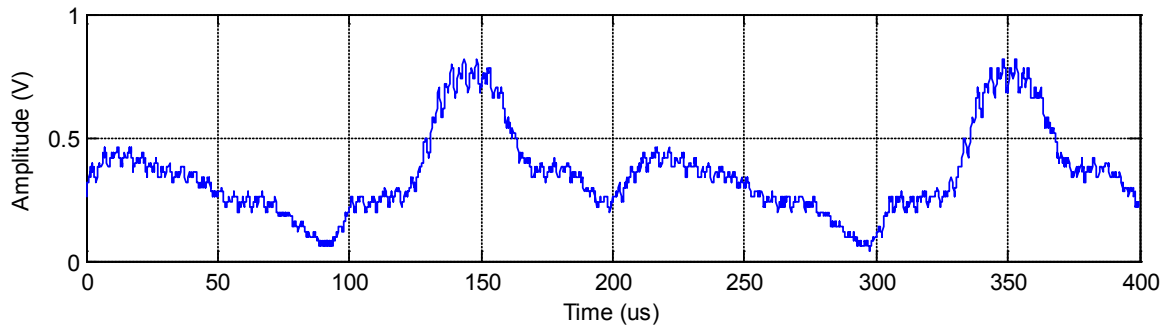


**Figure 4-13: Final output of the signal conditioning circuit**

The complete signal conditioning circuit uses a total of 3 ICs, and 20 passive components. This makes it very low cost per node, and can be fabricated quite compactly. A complete setup along with the signal conditioning circuit is depicted in Figure 4-14. A PCB layout of the SCC was also designed with dimensions similar to the TelosB mote, so that it can be stacked easily, as shown in Figure 4-15.

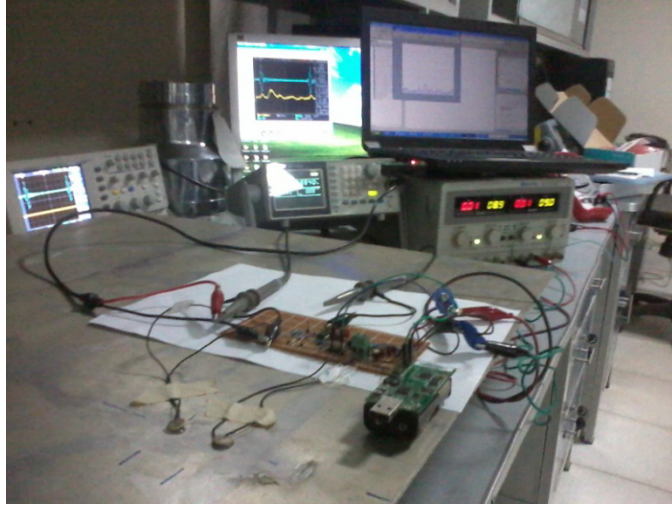


Figure 4-14: Complete test setup with signal conditioning circuit

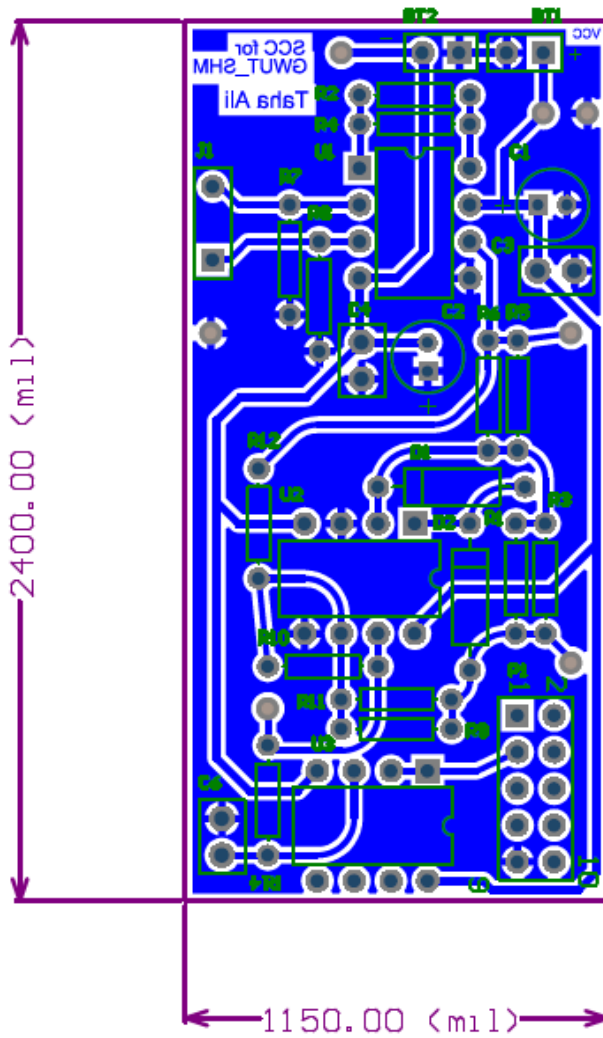


Figure 4-15: PCB layout design for the Signal Conditioning Circuit (SCC)

#### 4.4 Data Acquisition and Transmission over TelosB using TinyOS

To make GWUT based wireless SHM system a viable solution, the system has been designed using a low-power zigbee mote TelosB (MEMSIC TPR2420). The open-design wireless zigbee mote chosen, TelosB (MEMSIC TPR2420), was designed and developed by University of California, Berkeley (UCB). It aims large-scale, low-power sensing research, and runs open-source TinyOS, also designed by UCB. It has a high wireless transmission data rate of 250kbps, and operates in 2.4 GHz ISM band, which is truly universal. It has an on-board antenna, which provides a range of 100m outdoor. The on-board digital signal controller MSP430F1611 possesses 10 kB of on-chip RAM, and many useful embedded peripherals such as 12-bit ADC, DMA, dual 12-bit DAC, two USARTs and two 16-bit timers. The mote runs the open-source TinyOS, which is designed for low-power, practical embedded solutions. TinyOS runs programs written in NesC language, which provides an event-driven programming environment [18]. NesC, despite being a derivative of C, strictly enforces application-specific, component-oriented design to provide the desired reliability. TinyOS, is not a full-fledged OS by definition, it possesses a minimum kernel of just 400 bytes including code and data, which executes tasks sequentially from a FIFO list. When the task list is empty, the TinyOS kernel puts the TelosB platform in sleep mote saving tremendous power – it has a sleep mode current consumption of just 5.1  $\mu$ A, and active mode current consumption of 1.8 mA.

For acquisition of the envelope extracted by SCC, the on-chip ADC has to be configured for maximum sampling rate and throughput. The output waveform of SCC thus sampled is then buffered and segmented into appropriate packets for wireless transmission to a different mote connected with the Base Station (BS) as shown in Figure 4-16.



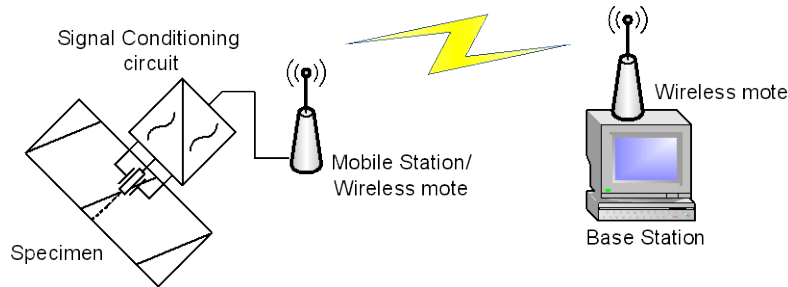


**Figure 4-16: Wireless SHM setup**

The ADC configuration, the communication protocols, and the state-diagrams are presented in the following sub-sections:

#### ***4.4.1 Implementation over NesC and TinyOS***

The NesC compiler is written to translate NesC code to C code with specific optimizations and checks; which is then compiled to object code by native C compiler of the respective platform. NesC has sophisticated but loosely defined three-layer hardware abstraction architecture. A Hardware Presentation Layer (HPL) provides direct access to all hardware registers through ‘get’ and ‘set’ commands. The Hardware Adaptation Layer (HAL), which sits on top of HPL, provides interfaces featuring complete functionality of different modular abstractions. Finally, a Hardware Interface Layer (HIL) provides hardware independent abstractions, which have been standardized and evolved within TinyOS community over time. A program written using only HIL abstractions will run on any TinyOS platform. However, HIL does not provide complete capability of the underlying hardware, because of the generalization. Therefore, one has to use a mix of HIL and HAL, or even HPL, to meet specific constraints. Thus, for meeting low power constraints along with high ADC sampling rates, the codes used in this study have to use a mix of HIL and HAL, also termed as weak HIL. That is, due to hardware

dependencies (high ADC sampling rates), the codes used in this study may target TelosB motes only, and may not run on other motes without modification.

The development was done by using Yeti2, an Eclipse IDE plug-in for TinyOS 2.x, over Ubuntu 12.04 OS (a GNU Linux flavor), because the NesC tools and TinyOS platform drivers are naturally developed for Linux, although development is possible over Windows via Cygwin. Yeti2 not only provides syntax highlighting and a modern editor with code completion etc., but also provides navigation via hyperlinks, component graphs, and an online preprocessor.

An application for TinyOS is usually written as a *configuration* (a wiring component), which consists of a *module* (an implementation component), wired to many other configurations or modules. These wirings are done through various *interfaces* defined either within components or separately. A component either *uses* or *provides* an interface. The component which provides an interface acts as the sink of commands over that interface, and provides the implementation of those commands. It may also signal *events* to the user component. The component which uses an interface has to implement all the events for that interface, and may *call* commands over it. For detailed understanding of the TinyOS programming, please refer to [18,19,20].

A typical component graph is shown in Figure 4-17. It shows how different modules and configurations are linked through interfaces, within an application's configuration. Figure 4-18 shows an expansion of the core application module depicting its interfaces, command functions and event functions in detail.

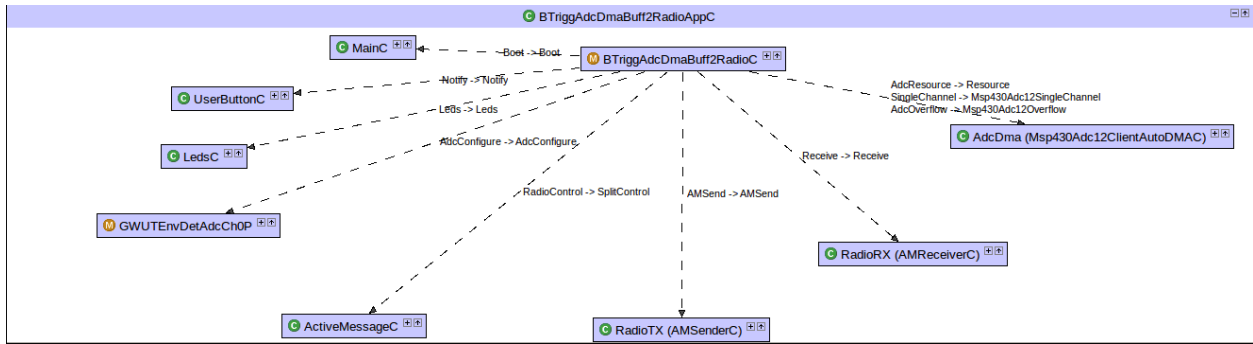


Figure 4-17: A component graph of a TinyOS application configuration in Yeti2

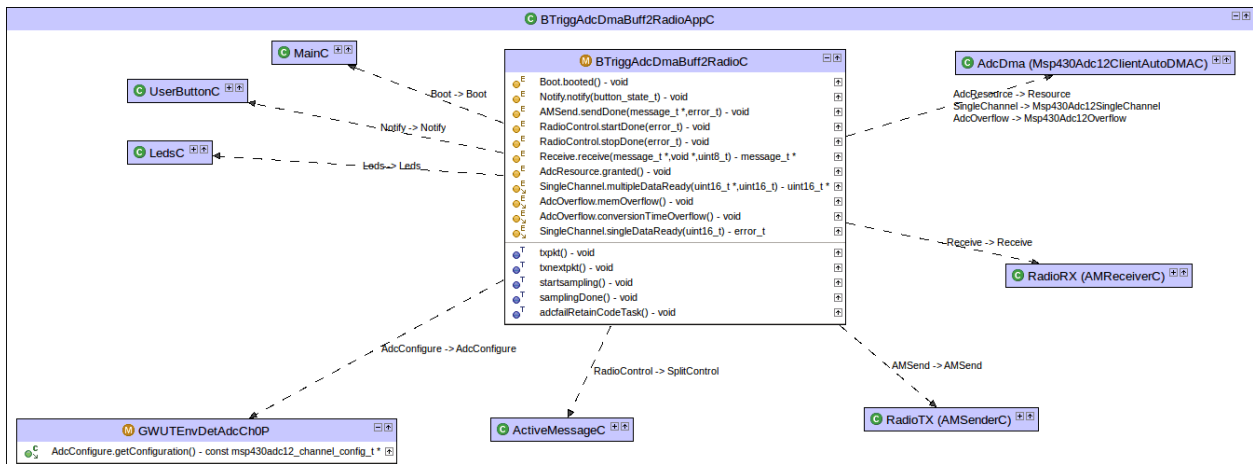


Figure 4-18: A component graph with module interfaces shown

#### 4.4.2 ADC configuration for TelosB

The TelosB's ADC is based on successive approximation conversion principle that needs a sample and hold circuit (S/H) at the input stage. The S/H circuit operates in two consecutive modes: sampling or following input signal and holding the signal value for conversion. To drive ADC at high sampling rates within acceptable error margins, the sample acquisition time should be kept minimal and at least match the sampling time of the S/H circuit. Sample acquisition time is defined as the time required for charging the capacitor of the S/H circuit in the following input mode. For MSP430F1611, it is defined in the datasheet as:

$$t_{\text{sample}} = \ln(2^{n+1})(R_s + R_i)C_i + 800 \times 10^{-9} \quad (9)$$

Where,  $n$  is the ADC resolution,  $R_s$  is the source resistance, and  $R_i, C_i$  are inherent input resistance and capacitance which are typically  $1\Omega$  and  $30\text{ pF}$  respectively. That is one of the reasons that the low pass filter was accompanied with a voltage follower, making it active low-pass filter, to keep the source resistance as low as possible thereby further reducing the sample acquisition time.

Now, the sampling time of the S/H circuit is determined by ADC12CLK. Master Clock (MCLK) was selected as the ADC12CLK through a divider set to 4 (minimum possible). MCLK is by default set to  $4\text{ MiHz}$  (MebiHertz<sup>3</sup>) in TinyOS. Thus, the ADC was configured for a sampling frequency of  $1\text{ MiHz}$  with appropriate sample acquisition time.

Furthermore, the Successive Approximation Register (SAR) core's conversion clock for the ADC is also configurable. SAR core was also driven by MCLK, with the divider set to 1. The S/H circuit takes one cycle of ADC12CLK to acquire the sample, and less than one cycle to synchronize with SAR core's conversion clock. After synchronization, the SAR core takes 13 cycles of MCLK to convert the analog value on hold to 12-bit code. Thus, the ADC was successfully configured for a sampling frequency of:

$$f_s = \left[ \left( \frac{2}{2^{20}} \right) + \left( \frac{13}{2^{22}} \right) \right]^{-1} = 199.73\text{ kps} \quad (10)$$

Since, the significant frequency content of the envelope is below  $80\text{ kHz}$  ( $0.4 \times 200\text{ kHz}$ ); a sampling rate around  $200\text{ kps}$  provides a ratio of 2.5, which satisfies the Nyquist criterion. However, practical reconstruction usually requires higher ratios, and depends upon the input signal's nature, but in our case, the Gaussian nature of the signal allows useful reconstruction.

Moreover, the overall ADC throughput should also match the sampling rate, that is, the sampled data in ADC's internal registers must be moved quickly enough to the main memory to

---

<sup>3</sup> Derived from the concept of Mebibyte ( $1\text{ MiHz} = 2^{20}\text{ Hz} = 1,048,576\text{ Hz}$ )  $\neq$  ( $1\text{ MHz} = 1,000,000\text{ Hz}$ )

avoid loss of data due to overwrites. The internal 16 registers of MSP430F1611's ADC fill fast with 16 consecutive samples, but each word (16-bit) takes 8 cycles of the CPU for a complete move to main memory (RAM). Because each sample is stored as a complete word, this copying time totals to  $8 \times 16 = 128$  cycles = 30.518 us, which is large comparable to the sampling time of 16 samples (80 us), causing jitters after every 32 samples in a saw-tooth wave due to missing samples as depicted in Figure 4-19. This was solved by configuring the DMA peripheral to transfer each word from the ADC's internal register to RAM, on each ADC sample interrupt. This took 2 cycles per word (477 ns) and was interleaved with the sampling time. Figure 4-20 shows a similar saw-tooth wave sampled using DMA. However, note that, the DMA peripheral in MSP430F1611 is not full-fledged; it stops CPU execution until all the samples have been transferred.

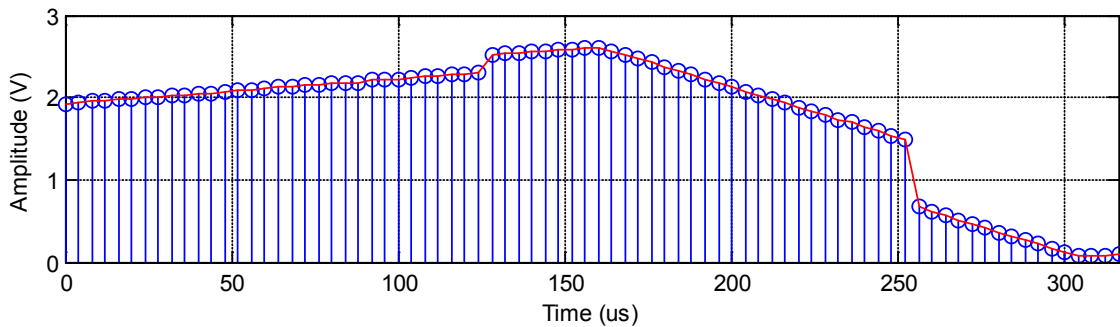


**Figure 4-19: Saw-tooth wave sampled without DMA**

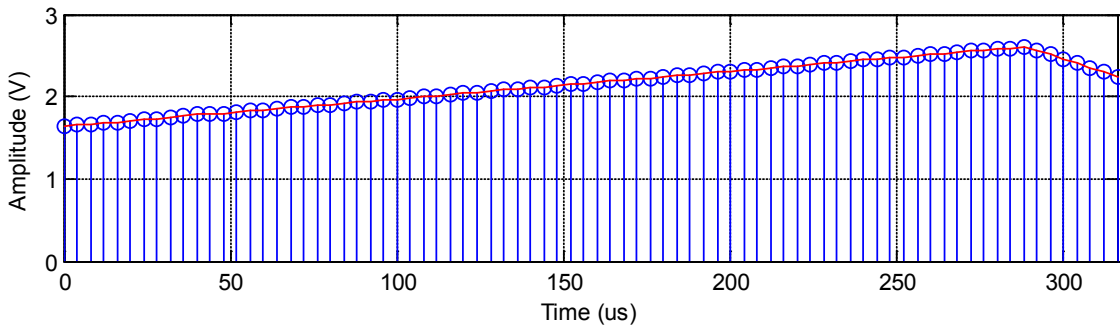


**Figure 4-20: Saw-tooth wave sampled with DMA**

### ***4.4.3 Wave capture and buffering***

As discussed earlier, the pulse was being repeated by the AFG at a regular repetition rate or PRF of 4.884 kHz. Therefore under steady state conditions, the received / sensed signal between two consecutive excitations, i.e. a single Pulse Repetition Interval (PRI), would be enough for comparison and subsequent fault detection. To capture one complete Pulse Repetition Interval (PRI), the sampling span was kept twice the PRI, i.e.  $2 \times \text{PRI} = 2/\text{PRF} = 409.5 \mu\text{s}$ . Therefore, if  $2 \times \text{PRI}$  is sampled at 200 ksps, then the number of samples that will cover the sampling span should be  $2 \times 200\text{k} \times 204.75\mu = 81.9 \approx 82$  samples.

However, the actual incoming rate of the sensed / received signal through a 12-bit ADC comes out to be  $12 \times 200 \text{ ksps} = 2400 \text{ kbps}$ . Whereas, the maximum outgoing wireless transmission data rate of TelosB mote is 250 kbps. That is, the sensed signal cannot be acquired and transmitted in real time. Therefore, the signal was buffered at the mote after acquisition. Now, the size of this buffer needs to be estimated before hand, because nesC does not allow dynamic memory allocation. Pre-allocation of memory makes the code application-specific but enhances reliability in unattended environments. As each 12-bit sample is stored and manipulated in a 16-bit register or word, an approximate 80 samples will require 160 bytes buffer for storing one complete sampling span.

### ***4.4.4 Communication protocol and packet format***

To wirelessly transmit data, single hop networking was considered. This can be easily extended to multi-hop networking scheme, if required, for large-scale wireless GWUT based SHM systems. The fundamental networking layer that is user-accessible in TinyOS is the Active Message Layer (AML) [19]. ‘message\_t’ is a standard message buffer of the AML. In essence, it

is a data link layer packet incorporating device-dependent parameters, and providing platform-independent access to layers above it. The header, footer and metadata fields are device-dependent whereas the data field is accessible by application layers above it. The data field has a maximum size, optimized to 28 bytes.

Moreover, the data transmitted wirelessly to the base station should be able to be reconstructed into the waveforms precisely for further processing. Thus, a custom format for the GWUT acquisition file has been designed, as shown in Figure 4-21. A customary one byte header and footer mark the start and end of the file respectively. An error byte indicates any configuration or sampling issues. The actual number of samples read is communicated by a two byte field, which may be less than 80 in case of a sampling error. To reconstruct the waveform appropriately, a four byte field conveys the inter-sample interval, i.e. interval between two consecutive samples. Finally, the sampled data field contains the 160 byte data, totaling the GWUT file size to 169 bytes. Other parameters, such as supply voltage are fixed and were fed to the BS program directly.

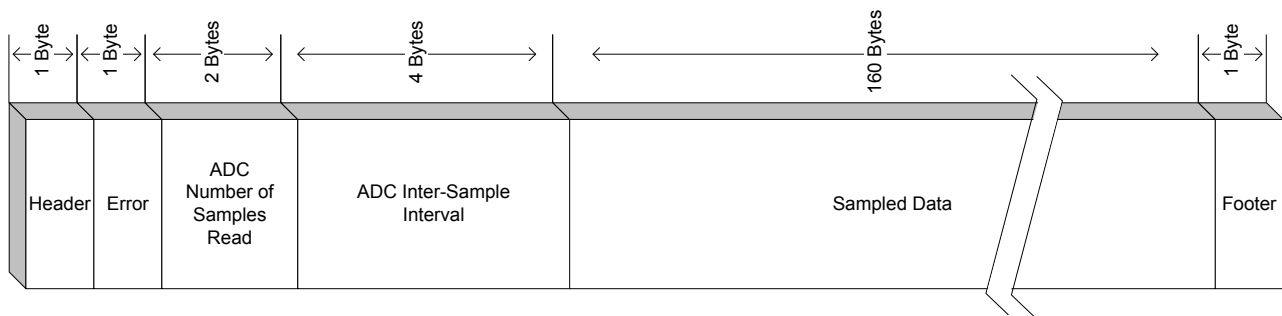


**Figure 4-21: GWUT acquisition file format**

Since the maximum size of the data field for 'message\_t' buffer is 28 bytes, one needs to transmit the GWUT acquisition file in packets. Therefore, the file was segmented into custom sequences (or packets) as shown in Figure 4-22.

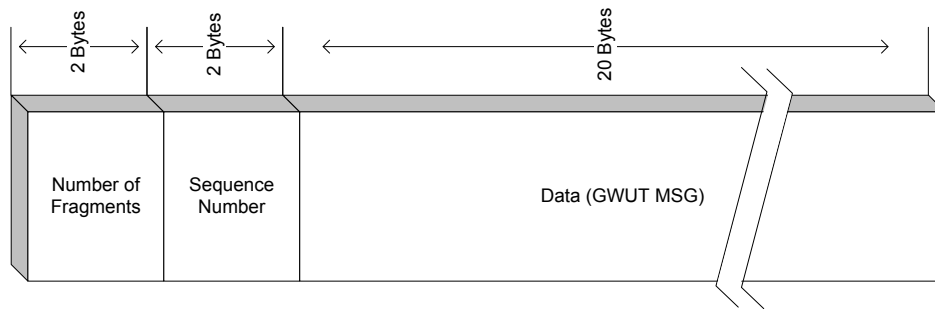


**Figure 4-22: GWUT data packet (sequence)**

Further, to keep things simple, the stop and wait protocol for single-hop communication was adapted. A protocol sequence diagram is presented in Figure 4-23.

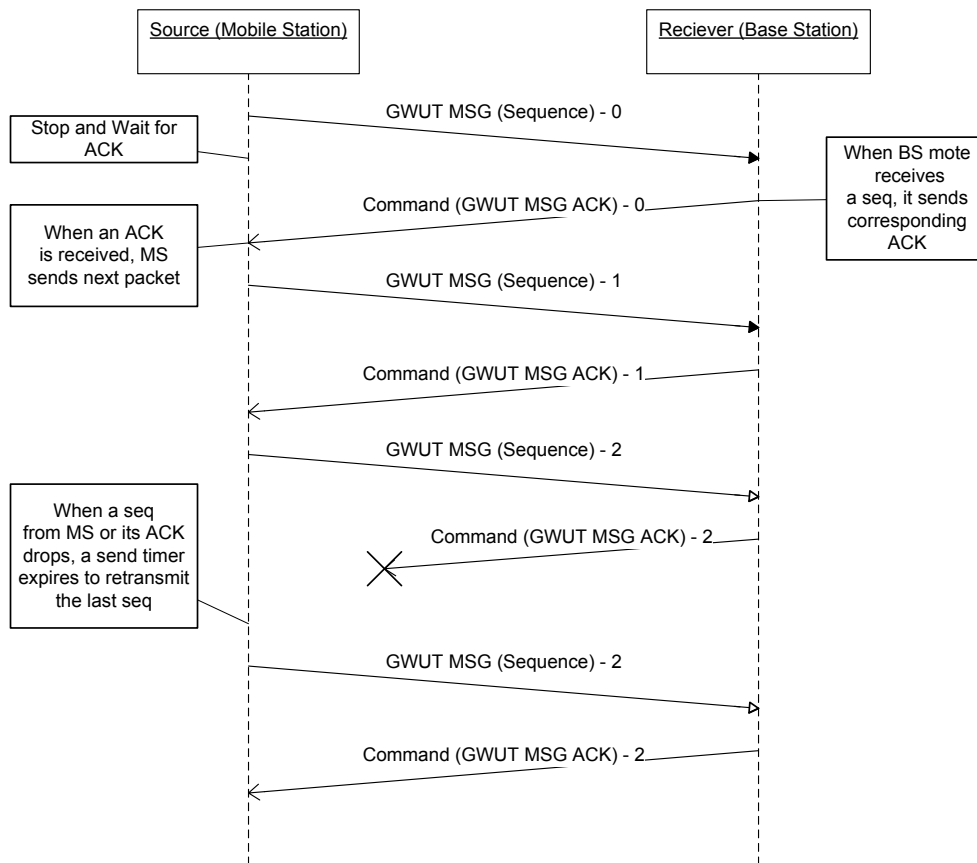


**Figure 4-23: Protocol sequence diagram implemented for Single-hop communication**

The commands depicted in Figure 4-23 were mainly acknowledgements of the GWUT data packets received at the BS. However, these were named as command packets because they were designed in a multipurpose format, and were also used to issue commands such as to start



sampling, start wireless transfer etc. for the Remote Station (RS), at a given instant. The commands were interpreted by the current state of the system and by two 2-byte optional parameters, as shown in Figure 4-24.

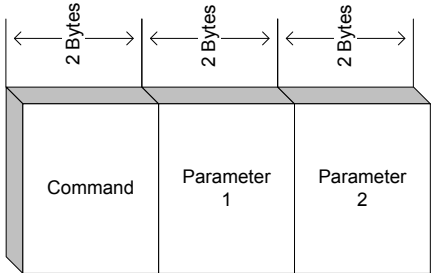
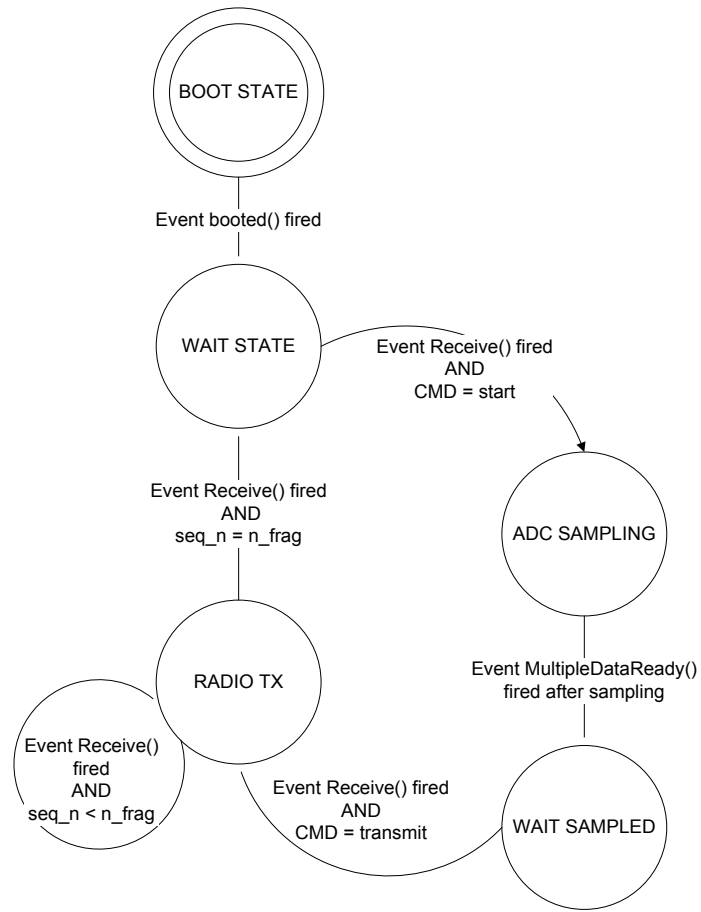


Figure 4-24: GWUT command and acknowledgement packet

**4.4.5 Program structure for remote station**

The remote wireless mote or RS was programmed to get the envelope of the sensed signal extracted by the SCC, and wirelessly transmit it to the BS, when commanded. This was done according to the formats defined earlier. The states of the program written for the mote at RS are depicted as a state diagram in Figure 4-25.



**Figure 4-25: State diagram for wireless mote at RS**

The wireless transmission was carried out according to the protocol defined earlier, for which the flow chart is illustrated in Figure 4-26.

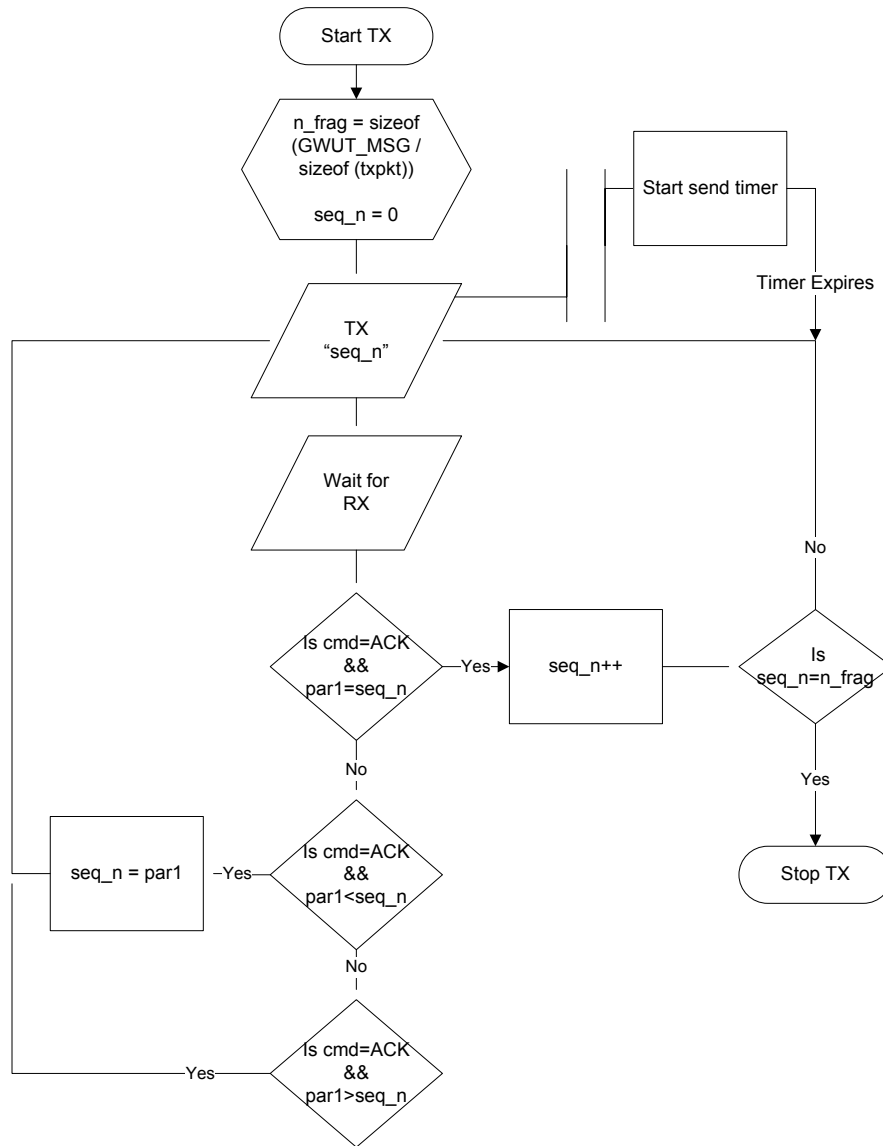


Figure 4-26: Transmission flow chart at RS mote

#### 4.4.6 Program structure for base station

The BS comprised of a wireless mote and a computer interfaced through an asynchronous serial port, operating at 115200 baud. The BS mote was programmed to convey the commands generated by the User Interface (UI) running at the BS computer, and download the GWUT acquisition file when needed. The UI was programmed to connect to and communicate with the

BS mote, reconstruct the signal waveforms and process them further for fault detection, offline.

The state diagram in Figure 4-27 depicts the behavior of BS mote program.

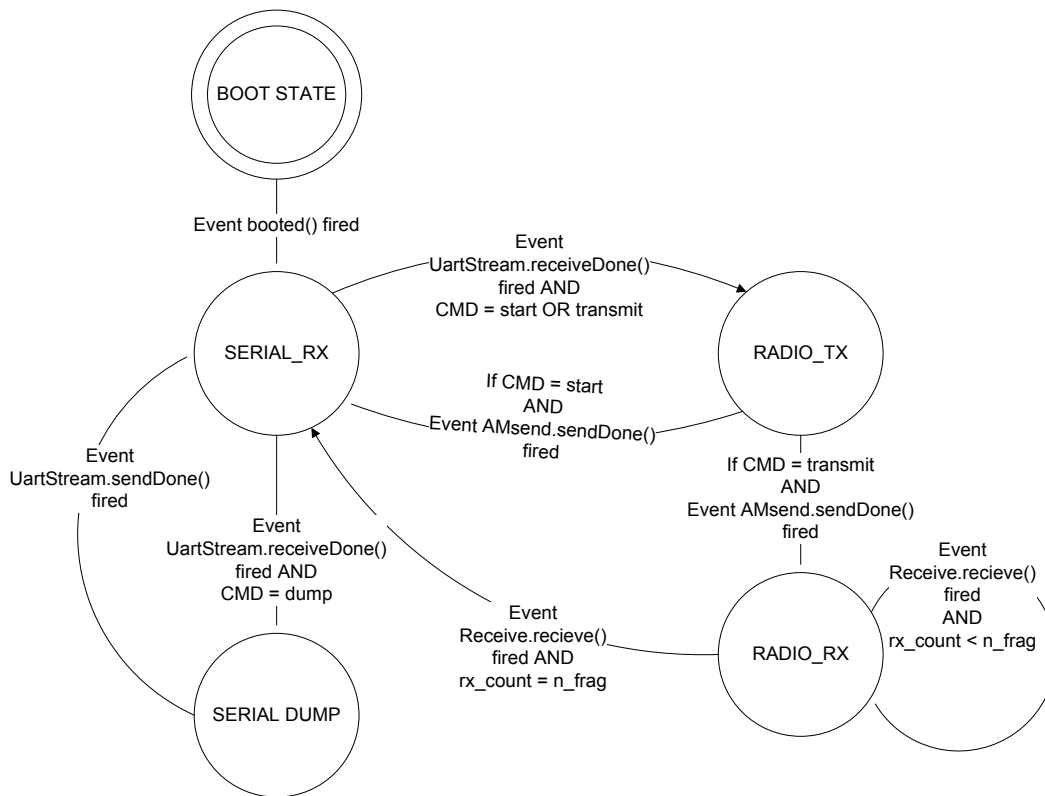


**Figure 4-27: State diagram for BS mote**

The wireless reception was carried out according to the protocol, for which the flowchart is illustrated in Figure 4-28.

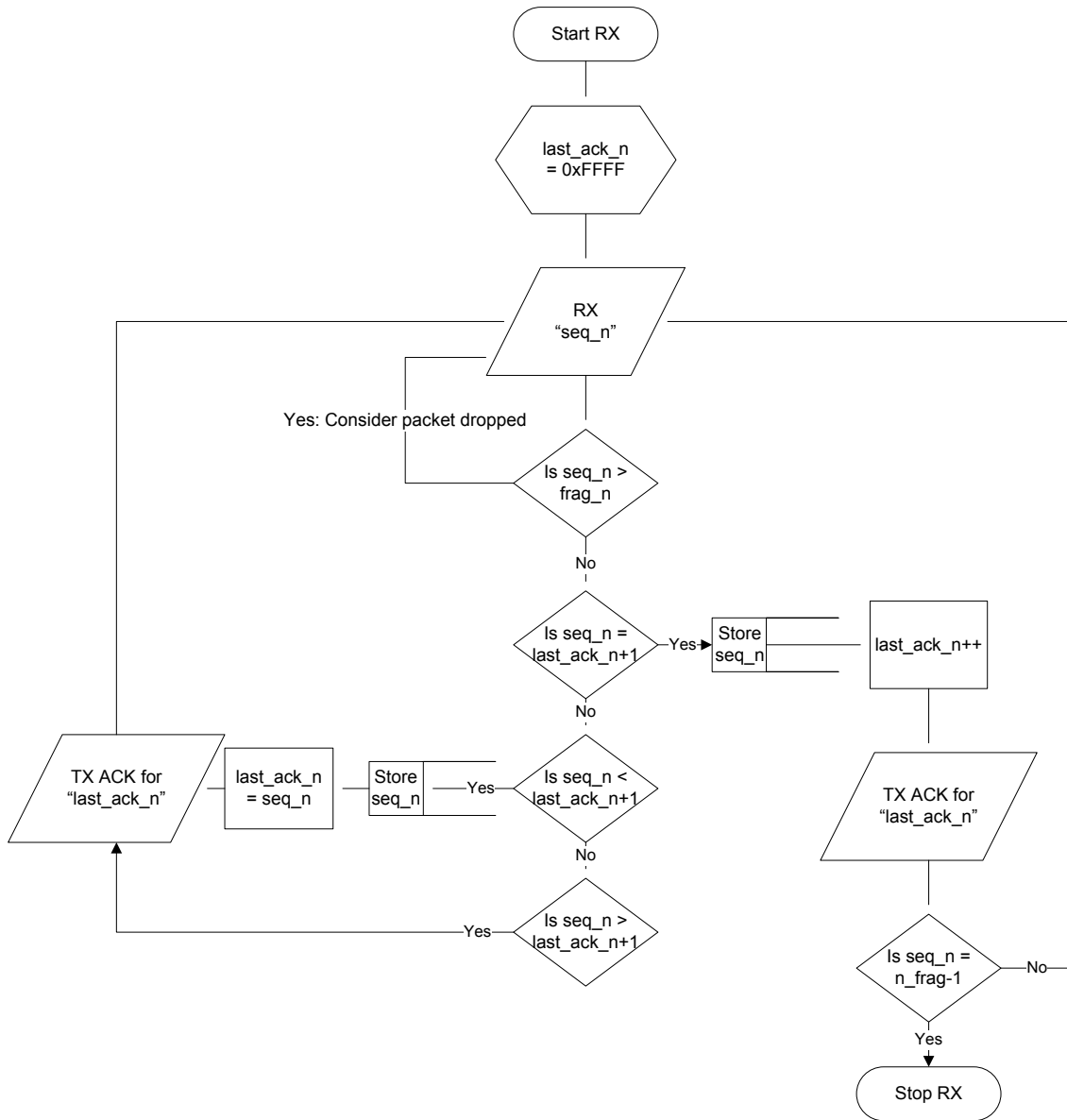


**Figure 4-28: Flowchart for reception at BS mote**

The UI running at the BS works by parsing the parameters and data from the GWUT acquisition file, and reconstructing the time-domain waveform. A typical converted time-domain waveform is shown in Figure 4-29, without further processing. However, this signal can't be directly used for flaw detection in a wireless GWUT-SHM system because of low resolution, but it provides a fair representation of the envelope extracted by the SCC. To increase the resolution, the signal was interpolated, as described in the next section.

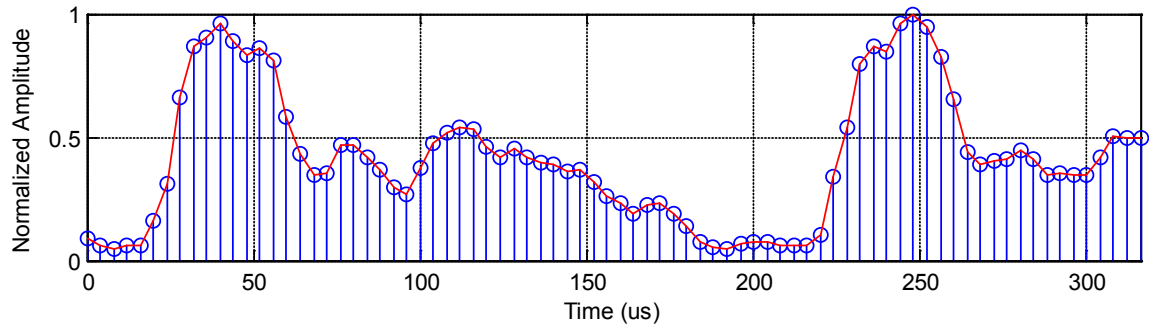


Figure 4-29: GWUT waveform acquired at BS

#### 4.5 Signal Processing at the Base Station

After retrieval and successful reconstruction at the BS, the signal's resolution was increased by decreasing the sample interval to  $1 \times 10^{-7}$  seconds using the 'spline' interpolation, a type of cubic piece-wise polynomial interpolation, for fair processing. This resulted in a signal, as shown in Figure 4-30, very similar to the original signal's envelope.

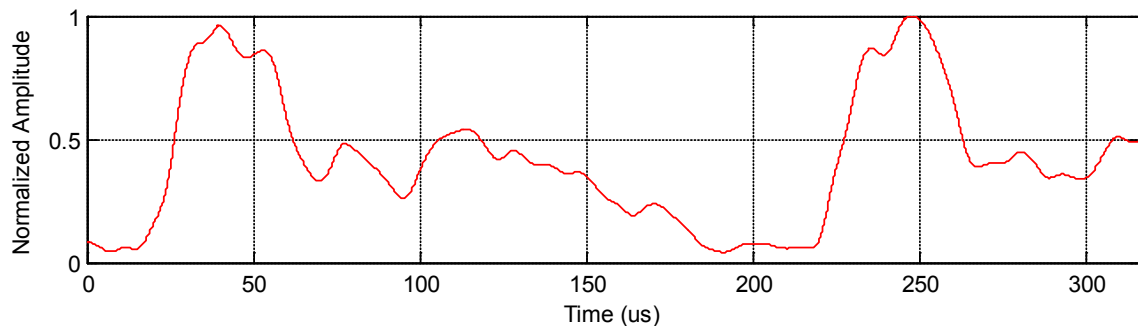


Figure 4-30: GWUT waveform after interpolation at BS

Now, the signal can be saved or further processed for flaw detection. This work uses differential signal processing techniques to classify a signal as 'healthy' or 'flawed' by comparison with a reference signal. A signal taken off a healthy plate was saved as a reference signal at the BS. Many complex algorithms can be followed for comparison of GWUT signals, which are discussed in the contemporary literature [11,17,21]. This work has followed a very

basic comparison method based on subtraction of the incoming signal from reference signal after normalization and *registration*. This is followed by thresholding to classify the signals.

Both signals were normalized by their peak values. Signal registration mainly includes the alignment of an observed signal with a reference signal. The registration algorithm used in this work was feature based rather than statistical. It worked by isolating the peaks in the observed or reference signal corresponding to the two excitation-peaks that are present in one sampling span. The peaks were isolated based on their normalized amplitude and distance between them. Then, the two signals were aligned for approximately one PRI span between the peaks at a time registered for the first peak. Now, because the region of interest lies in the center of the two peaks, the portion (60% of registered length) was windowed for comparison. Relative energy for the windowed difference signal was computed and used for classification as presented in the next section.

## 4.6 Results

An arbitrary signal taken off the healthy specimen with previously described setup and retrieved wirelessly through the SCC was saved as the reference signal for this setup at the BS. This reference signal is shown in Figure 4-31 after interpolation, normalization and registration.

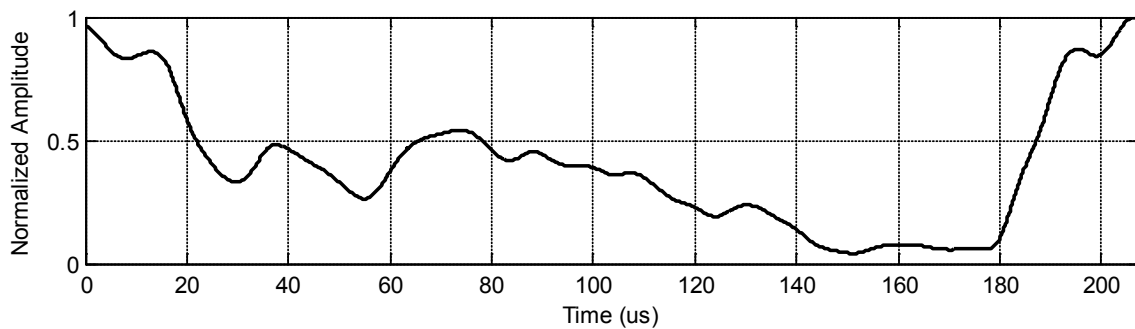


Figure 4-31: Reference signal (healthy) after registration

Figure 4-32 and Figure 4-33 present two healthy signals compared after registration at the BS. All signals were successfully registered with a minimum peak height of 0.9 or 90% and minimum peak distance of  $1.7 \times 10^{-4}$  s. Note that the signal Healthy-2 was not registered perfectly, because it didn't captured complete PRI after the first peak but captured enough to fulfill the registration criteria.

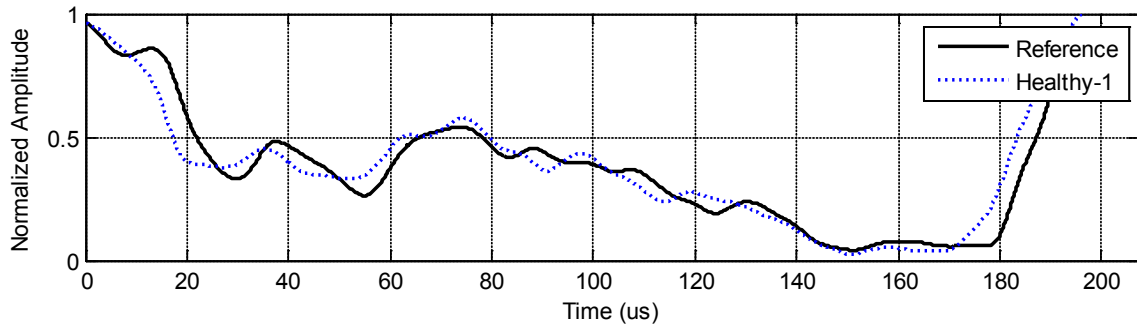


Figure 4-32: Signal Healthy-1 compared with reference at BS

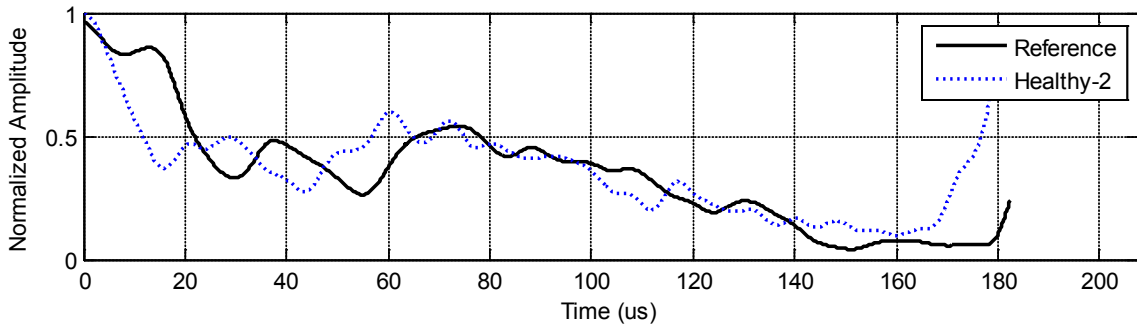


Figure 4-33: Signal Healthy-2 compared with reference at BS

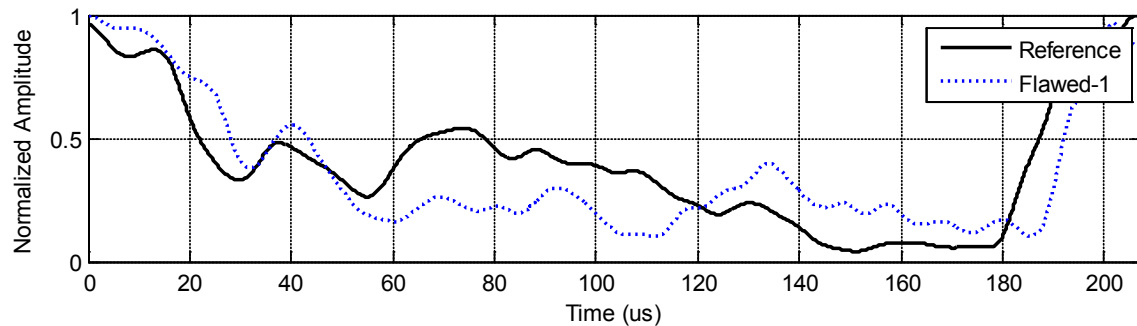


Figure 4-34: Signal Flawed-1 compared with reference at BS



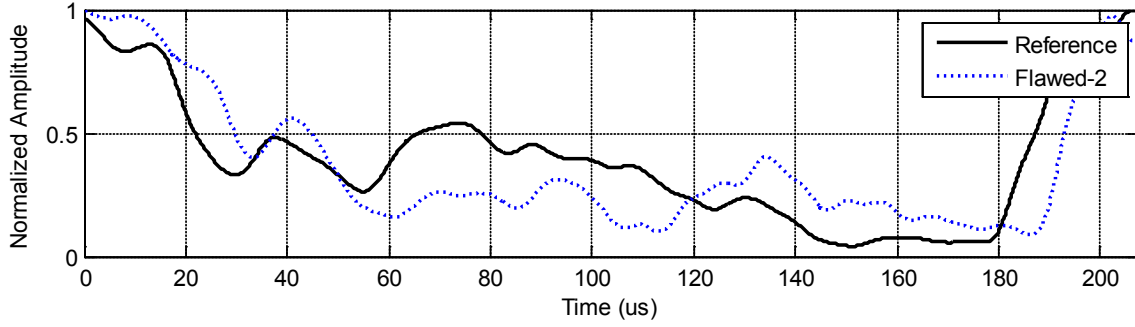


Figure 4-35: Signal Flawed-2 compared with reference at BS

Similarly, two signals taken off flawed specimen with the same setup are compared with the reference in Figure 4-34 and Figure 4-35. Now, relative energies for each signal were computed as follows:

$$RE = \frac{\sum_i x_i^2}{\sum_i r_i^2} \times 100 \quad (11)$$

Where ‘x’ is the difference signal, ‘r’ is the reference signal and ‘i’ represent the set of indices of the window. The values are tabulated in Table 1.

Table 1: Relative energies of difference between windowed reference and target signals

Signal	RE
Healthy-1	1.373%
Healthy-2	5.597%
Flawed-1	28.6312%
Flawed-2	26.8431%

Thus, an appropriate threshold, say 10%, can be easily used to identify flaws. Finally, a wireless low-power GWUT based SHM system design has been presented for an excitation frequency of 200 kHz, and with a lowered sampling rate of 200 kps. The transmission data volume is also reduced to 169 bytes for an acquisition span of 409.5 μs.

## Chapter 5 Discussion and Future Work

---

### 5.1 Defense of Thesis – Comparison with Contemporary work

This research work has presented a novel low-power wireless sensing system design for GWUT based SHM, by reducing the sampling rate requirement and transmission data volume. The design presented bears less weight and is cost-effective per node as compared to the contemporary designs. It uses only 3 inexpensive ICs and 20 passive components, besides a transducer at each wireless node, where a zigbee mote serves as a Remote Station (RS). The SCC was successfully designed to differentially sense the signal from the piezoelectric transducer and extract its envelope, which can be sampled by the mote's ADC and subsequently registered by the BS. The envelope of the sensed signal provided the requisite information at a much lower sampling rate given the excitation-signal's frequency. By transmitting the envelope instead of the complete signal also reduced the transmitted data volume, and was successfully used for flaw detection at the BS, as indicated by the results presented in the previous chapter.

However, many statistical approaches and complex algorithms can be utilized for precise flaw detection, flaw characterization or severity measurements. These advanced signal processing techniques are already discussed in the literature [11,17,21]. Notable statistical features include normalized short-time cross-correlation in a specific time-span, total curve length, and higher order statistical parameters. These features can be used to train a suitable classifier for precise flaw detection and characterization. Nevertheless, the relative energy feature was enough to demonstrate system's capability for GWUT based SHM at par.

**Table 2: Comparison with state-of-the-art wireless GWUT-SHM systems**

Specifications	This Work	Zhao et al.	Pertsch et al.	Dib et al.
Excitation frequency for GWUT	200 kHz	350 kHz	1 MHz	75 kHz
Computing core	Digital Signal Controller	Mixed Signal Microcontroller	Digital Signal Processor	Microcontroller
Processor number and placement	MSP430F1611, On-mote	C8051F120, External	TMS320F28335, On-board an external Kit	Atmega 1281, On-mote
ADC resolution and placement	12-bit ADC, On-chip	8-bit external ADC1173	12-bit ADC, On-chip	10-bit ADC, On-chip
ADC sampling rate	200 ksps	10 Msps	8.3334 Msps	273 ksps
Memory	(48 kB + 256 B) Flash, On-chip +10 kB RAM, On-chip +1 MB Flash, On-mote	128 kB Flash, On-chip + (8 kB + 256 B) RAM, On-chip	512 kB Flash, On-chip + 68 kB RAM, On-chip + 256 kB RAM, On-board	128 kB Flash, On-chip +8 kB RAM, On-chip +512 kB Flash, On-mote
Number of bytes transmitted for each acquisition	169 B	~4000 B	> 140 B	> 5000 B
Single acquisition time	409.5 $\mu$ s	NA	8 $\mu$ s	9.15 ms
Power consumption (stand-by) <sup>a</sup>	66.6 mW [66.6m (SCC) + 15.3 $\mu$ (mote)]	81.4 mW <sup>b</sup> [60m ( $\mu$ C) + 20.9m (ADC) + 0.27m (TX) + 0.25 (RX)]	199mW [15.5m ( $\mu$ P) + 66m (SRAM) + 66u (RF) + 117m (SCC)]	33 $\mu$ W
Power consumption (active mode) <sup>a</sup>	130.28 mW [66.6m (SCC) + 63.68m (mote)]	194 mW <sup>b</sup> [110m ( $\mu$ C) + 32.8m (ADC) + 21m (TX) + 30m (RX)]	1.24 W [712m ( $\mu$ P) + 248m (SRAM) + 165m (RF) + 117m (SCC)]	72.76 mW
Wireless data rate	250 kbps	56 kbps	38.4 kbps	250 kbps

<sup>a</sup> Power consumption is estimated as a product of typical supply voltage and current, for sensing chain of the platforms only

<sup>b</sup> Assuming processor clock frequency of 50 MHz

SCC = Signal Conditioning Circuit, TX = transmitter, RX = Receiver

Table 2 illustrates the detailed specifications of the sensing chain of the system design presented in contrast with the contemporary systems reported specifically for GWUT. It is evident that the designed system has lower power consumption for both stand-by and active modes and lower sampling rate as compared to Zhao et al. and Pertsch et al., while operating at the desired excitation frequencies for GWUT in hundreds of kHz. Only the system designed by Dib et al. consumed less power and used a comparable sampling rate, but on the expense of low excitation frequency, i.e. 75 kHz. Further, their transmission data volume was far greater than this work. Transmission of envelope instead of the complete sensed signal caused enormous

reduction in data volume – 169 bytes per sampling span length of 409.5  $\mu\text{s}$  against more than 140 bytes per sampling span length of just 8  $\mu\text{s}$  by Pertsch et al. Note that, the SCC was powered with a dual supply of  $\pm 9\text{V}$  through batteries, for this work. Thus, replacing current components in SCC with equivalent single-supply and rail to rail operating ones can further lower the power consumption and weight of the system.

Moreover, the stand-by power can be dropped to just that of the wireless mote by installing a relay for the supply of SCC controlled by the mote. This will result in tremendous power savings, yielding a stand-by power of 15.3  $\mu\text{W}$ , and stretching the recharge / maintenance cycles, because for a typical SHM system the active time is a very small fraction of the total life. The system turns active only for acquisitions, which may be a few times a day depending upon the requirements, and that's why lowering the transmission data volume was also desirable, because it reduces the active time of the system decreasing the power consumption.

## **5.2 Limitations**

Because specimen and transducers were not readily available, the research remained limited to detection of a particular flaw. However, this work mainly focused on enhancement of remote sensing system for GWUT based SHM. Further, the Arbitrary Function Generator (AFG) used in this work doesn't intrinsically support single pulse excitation for arbitrary waveforms. Therefore, the excitations were made repeatedly at a PRF of 4.884 kHz. For a fair comparison, all acquisitions were made amid steady-state excitations. However, the PRI was set as to receive the A0 mode echoes at the sensor PZT from a distance greater than 10 cm, without distorting excitation-signal resolution. The PRI can be increased on the expense of decreased output sample rate of the AFG, for better sensitivity in long range GWUT. Nevertheless, the system design

presented is equally applicable for single pulse excitation and single transducer pulse-echo. The sampling span can also be easily increased for long range applications.

The current hardware design of SCC supports a maximum frequency of 200 kHz, because of the slew rate limitation of the IA. This can be easily enhanced by replacing the IC for IA with one bearing better specifications. Another approach is to reduce the voltage gain being taken from the IA, lowering the required slew rate, and either use an additional wide-band amplifier or increase the gain from the weighted summer circuit. Further, the SCC performance can be improved by using resistors with better tolerance, because the precision rectifier circuit needs perfectly matched resistor values for ideal operation; current work uses 1% resistors.

### **5.3 Conclusion**

The use of hardware based envelope detection is a novel contribution in wireless GWUT based SHM systems. It paves the way for low-power remote sensing, which makes this system practically feasible to be implemented on large scales. The solution not only reduces power consumption but also reduces the cost and weight of the modules per node. Further, it breaks the conventional constraints of high sampling rates and transmission data volume associated with GWUT based SHM systems, enabling low-power and low-cost wireless instrumentation.

All implementation details are presented and discussed in appropriate depth along with the requisite theoretical background and literature survey. To conclude, an efficient, low power, remote sensing system design is proposed for a wireless GWUT based SHM system that has applications for aerospace as well as civil structures.

## **5.4 Summary of Contributions**

Following is a list of accomplishments resulted from this work, including but not limited to:

1. For the first time in Pakistani academia, research on instrumentation design for GWUT has been attempted. This has resulted in a foundation for further research and development in this area.
2. An inter-disciplinary research area has been explored in an appropriate depth required for Masters level degree, for practical solutions to real problems.
3. A complete wireless GWUT-SHM system prototype has been developed, which can easily be readily converted to a domestic business product for Pakistan, saving foreign exchange and possible life or property damages. With careful entrepreneurship, the sale of the product may return surplus revenue through exports.
4. A novel design for low-power sensing in wireless GWUT-SHM has been proposed, as a universal contribution.

## **5.5 Recommendations for future work**

The experimental setup can be modified and further tuned to excite only a single non-dispersive mode as discussed in the literature review. Moreover, better couplants such as cyanoacrylate should give better results. Furthermore, Finite Element Modeling (FEM) of the experiments conducted will help in tuning various parameters for further optimization. It will also help to understand the behavior of the specimen and PZT wafers under different set of conditions.

On-mote generation of excitation signal can be done using the on-chip DAC and some external circuitry. Further, the pair of transducer can be replaced by a single transducer that will act as both an actuator and sensor (true transducer). This may require an analog multiplexer / demultiplexer controlled by the mote.

Another interesting advancement will be to implement some basic signal processing algorithms at the mote end, making it smart by reducing the transmission data volume even further. Finally, using PZT arrays for flaw localization and characterization leading to a large-scale implementation is an obvious extension of the current work.

## References

- [1] H Assler and J Telgkamp, "Design of aircraft structures under special consideration of NDT," *9th ECNDT, September*, pp. 25-29, 2006. [Online]. [http://ultraligero.net/Cursos/disenio/Design\\_Of\\_Aircraft\\_Structures\\_Under\\_Special\\_Consideration\\_NDT.pdf](http://ultraligero.net/Cursos/disenio/Design_Of_Aircraft_Structures_Under_Special_Consideration_NDT.pdf)
- [2] Jerome P Lynch and Kenneth J Loh, "A summary review of wireless sensors and sensor networks for structural health monitoring," *Shock and Vibration Digest*, vol. 38, no. 2, pp. 91-130, 2006. [Online]. <http://abdaoui.free.fr/t/PostDocQatar2/Proposal/Documentations/SHM/10.1.1.126.6482.pdf>
- [3] Haitao Xiao and Harutoshi Ogai, "A distributed localized decision self-health monitoring system in WSN developed for bridge diagnoses," in *Communication Software and Networks (ICCSN), 2011 IEEE 3rd International Conference on*, 2011, pp. 23-28. [Online]. [http://ieeexplore.ieee.org/xpls/abs\\_all.jsp?arnumber=6013653](http://ieeexplore.ieee.org/xpls/abs_all.jsp?arnumber=6013653)
- [4] KC Lu et al., "Application of wireless sensors for structural health monitoring and control," in *Proceedings of KKCNN Symposium on Civil Engineering, Taiwan*, 2005. [Online]. [http://wang.ce.gatech.edu/publication\\_pdfs/Conference\\_Papers/KKCNN-Wireless%20Sensor.pdf](http://wang.ce.gatech.edu/publication_pdfs/Conference_Papers/KKCNN-Wireless%20Sensor.pdf)
- [5] Victor Giurgiutiu, "Embedded ultrasonics NDE with piezoelectric wafer active sensors," *Journal Instrumentation, Measure, Metrologie, Lavoisier Pub., Paris, France, RS series M*, vol. 12, pp. 3-4, 2003. [Online]. [http://www.me.sc.edu/research/lamss/pdf/journals/37\\_lavoisier\\_imm\\_12m\\_v3\\_n3-4\\_2003\\_pp149-180.pdf](http://www.me.sc.edu/research/lamss/pdf/journals/37_lavoisier_imm_12m_v3_n3-4_2003_pp149-180.pdf)
- [6] Albert S. Buirks, Robert E. Green Jr., and Paul McIntire, *Nondestructive Testing Handbook, Volume 7, Ultrasonic Testing*, 3rd ed., Paul McIntire, Ed.: American Society of Nondestructive Testing, 2007, vol. 7. [Online]. <https://www.asnt.org/Store/ProductDetail?productKey=33b38755-1b19-47b0-b423-7ff24f847ecc>
- [7] Victor Giurgiutiu, "Lamb wave generation with piezoelectric wafer active sensors for structural health monitoring," in *Smart Structures and Materials*, 2003, pp. 111-122. [Online]. <http://proceedings.spiedigitallibrary.org/proceeding.aspx?articleid=761073>
- [8] Alexander Pertsch, Jin-Yeon Kim, Yang Wang, and Laurence J Jacobs, "An intelligent stand-alone ultrasonic device for monitoring local structural damage: implementation and preliminary experiments," *Smart Materials and Structures*, vol. 20, no. 1, p. 015022, 2011. [Online]. [http://wang.ce.gatech.edu/publication\\_pdfs/Wireless\\_Ultrasonic\\_2ndSubmission.pdf](http://wang.ce.gatech.edu/publication_pdfs/Wireless_Ultrasonic_2ndSubmission.pdf)
- [9] Jian Wu et al., "Multi-agent system design and evaluation for collaborative wireless sensor network in large structure health monitoring," *Expert Systems with Applications*, vol. 37, no. 3, pp. 2028-2036, 2010. [Online]. <http://www.sciencedirect.com/science/article/pii/S0957417409006435>
- [10] Sukun Kim et al., "Health monitoring of civil infrastructures using wireless sensor



- networks," in *Information Processing in Sensor Networks, 2007. IPSN 2007. 6th International Symposium on*, 2007, pp. 254-263. [Online]. [http://ieeexplore.ieee.org/xpls/abs\\_all.jsp?arnumber=4379685](http://ieeexplore.ieee.org/xpls/abs_all.jsp?arnumber=4379685)
- [11] Jennifer E Michaels and Thomas E Michaels, "Ultrasonic signal processing for structural health monitoring," in *AIP Conference Proceedings*, 2003, pp. 1476-1483.
- [12] Xiaoliang Zhao et al., "Active health monitoring of an aircraft wing with an embedded piezoelectric sensor/actuator network: II. Wireless approaches," *Smart materials and structures*, vol. 16, no. 4, p. 1218, 2007. [Online]. <http://iopscience.iop.org/0964-1726/16/4/033>
- [13] G. Dib et al., "Wireless NDE sensor system for continuous monitoring," in *AIP Conference Proceedings*, vol. 1335, 2011, pp. 1758-1765. [Online]. <http://scitation.aip.org/content/aip/proceeding/aipcp/10.1063/1.3592141>
- [14] Horace Lamb, "On waves in an elastic plate," *Proceedings of the Royal Society of London. Series A*, vol. 93, no. 648, pp. 114-128, 1917. [Online]. <http://rspa.royalsocietypublishing.org/content/93/648/114.full.pdf>
- [15] JH Nienwenhui, John J Neumann Jr, David W Greve, and Irving J Oppenheim, "Generation and detection of guided waves using PZT wafer transducers," *Ultrasonics, Ferroelectrics and Frequency Control, IEEE Transactions on*, vol. 52, no. 11, pp. 2103-2111, 2005.
- [16] Hai-Yan Zhang and Jian-Bo Yu, "Piezoelectric transducer parameter selection for exciting a single mode from multiple modes of Lamb waves," *Chinese Physics B*, vol. 20, no. 9, p. 094301, Sep 2011.
- [17] Jennifer E Michaels, "Detection, localization and characterization of damage in plates with an in situ array of spatially distributed ultrasonic sensors," *Smart Materials and Structures*, vol. 17, no. 3, p. 035035, 2008. [Online]. <http://iopscience.iop.org/0964-1726/17/3/035035>
- [18] David Gay et al., "The nesC language: A holistic approach to networked embedded systems," in *ACM Sigplan Notices*, vol. 38, 2003, pp. 1-11. [Online]. <http://www.tinyos.net/dist-2.0.0/tinyos-2.0.0beta1/doc/nesc/ref.pdf>
- [19] Philip Levis and David Gay, *TinyOS programming.*: Cambridge University Press, 2009.
- [20] Philip Levis et al., "TinyOS: An operating system for sensor networks," in *Ambient intelligence.*: Springer, 2005, pp. 115-148. [Online]. <http://www.itu.dk/people/rialf04/Mote%20Sensor%20Network/IR-TR-2004-60-ai-bookchapter-tinyos.pdf>
- [21] James S Hall and Jennifer E Michaels, "Computational efficiency of ultrasonic guided wave imaging algorithms," *Ultrasonics, Ferroelectrics and Frequency Control, IEEE Transactions on*, vol. 58, no. 1, pp. 244-248, 2011. [Online]. [http://ieeexplore.ieee.org/xpls/abs\\_all.jsp?arnumber=5688419](http://ieeexplore.ieee.org/xpls/abs_all.jsp?arnumber=5688419)
- [22] Haitao Xiao et al., "The health monitoring system based on distributed data aggregation for WSN used in bridge diagnosis," in *SICE Annual Conference 2010, Proceedings of*, 2010, pp. 2134-2138. [Online]. <http://ieeexplore.ieee.org/stamp/stamp.jsp?arnumber=5603255>
- [23] H Speckmann and R Henrich, "Structural health monitoring (SHM)--overview on technologies under development," in *16th World Conference on NDT, Montreal/CDN*, 2004. [Online]. [http://www.ndt.net/article/wcndt2004/pdf/aerospace/563\\_henrich.pdf](http://www.ndt.net/article/wcndt2004/pdf/aerospace/563_henrich.pdf)
- [24] Joseph Polastre, Robert Szewczyk, and David Culler, "Telos: enabling ultra-low power

- wireless research," in *Information Processing in Sensor Networks, 2005. IPSN 2005. Fourth International Symposium on*, 2005, pp. 364-369.
- [25] Pedro Mar et al., "Integrated Electronic System for Ultrasonic Structural Health Monitoring," in *European Workshop on Structural Health Monitoring*, 2012. [Online]. <http://www.ndt.net/article/ewshm2012/papers/fr1c1.pdf>
- [26] Venkata A Kottapalli et al., "Two-tiered wireless sensor network architecture for structural health monitoring," in *Smart Structures and Materials*, 2003, pp. 8-19. [Online]. <http://proceedings.spiedigitallibrary.org/proceeding.aspx?articleid=761164>
- [27] James S. Hall and Jennifer E. Michaels, "A model-based approach to dispersion and parameter estimation for ultrasonic guided waves," *The Journal of the Acoustical Society of America*, vol. 127, no. 2, p. 920, 2010. [Online]. <http://dx.doi.org/10.1121/1.3273894>
- [28] "Low Cost Low Power Instrumentation Amplifier, AD620," Analog Devices, Datasheet AD620, Rev. H, 2011. [Online]. [http://www.analog.com/static/imported-files/data\\_sheets/AD620.pdf](http://www.analog.com/static/imported-files/data_sheets/AD620.pdf)
- [29] "Yeti 2 - TinyOS 2 Plugin for Eclipse IDE,". [Online]. <http://tos-ide.ethz.ch/wiki/index.php>
- [30] "TL082 Wide Bandwidth Dual JFET Input Operational Amplifier," Texas Instruments, Datasheet TL082, Nov. 2004.
- [31] "NDT Resource Center,". [Online]. <https://www.nde-ed.org/EducationResources/CommunityCollege/communitycollege.htm>
- [32] "TelosB Mote TPR2420," MEMSIC, Datasheet TPR2420CA, Rev A.
- [33] "TinyOS Enhancement Proposals (TEPs)," [Online]. <http://tinyos.stanford.edu/tinyos-wiki/index.php/TEPs>
- [34] "Tiny OS,". [Online]. <http://www.tinyos.net/>
- [35] "MSP430F15x, MSP430F16x, MSP430F161x Mixed Signal Microcontroller," Texas Instruments, Family Datasheet MSP430F1611, Mar. 2011.
- [36] "BAT42, BAT43 Small Signal Schottky Diodes," STMicroelectronics, Datasheet BAT42, Rev. 1C, Oct. 2001.